Monthly Notices
of the
ROYAL ASTRONOMICAL SOCIETY

MNRAS **436,** 2465–2483 (2013)
Advance Access publication 2013 October 11

doi:10.1093/mnras/stt1741

# Daily multiwavelength *Swift* monitoring of the neutron star low-mass X-ray binary Cen X-4: evidence for accretion and reprocessing during quiescence

F. Bernardini,[1,2]★ E. M. Cackett,[1] E. F. Brown,[3] C. D'Angelo,[4] N. Degenaar,[5]†
J. M. Miller,[5] M. Reynolds[5] and R. Wijnands[4]

[1]*Department of Physics & Astronomy, Wayne State University, 666 W. Hancock St., Detroit, MI 48201, USA*
[2]*INAF, Osservatorio Astronomico di Capodimonte, Salita Moiariello 16, I-80131 Napoli, Italy*
[3]*Department of Physics & Astronomy, National Superconducting Cyclotron Laboratory, Michigan State University, East Lansing, MI 48824, USA*
[4]*Instituut Anton Pannekoek, University of Amsterdam, NL-1098 XH Amsterdam, the Netherlands*
[5]*Department of Astronomy, University of Michigan, 500 Church St, Ann Arbor, MI 48109-1042, USA*

Accepted 2013 September 13. Received 2013 September 13; in original form 2013 July 9

## ABSTRACT

We conducted the first long-term (60 d), multiwavelength (optical, ultraviolet, UV, and X-ray) simultaneous monitoring of Cen X-4 with daily *Swift* observations from 2012 June to August, with the goal of understanding variability in the low-mass X-ray binary Cen X-4 during quiescence. We found Cen X-4 to be highly variable in all energy bands on time-scales from days to months, with the strongest quiescent variability a factor of 22 drop in the X-ray count rate in only 4 d. The X-ray, UV and optical ($V$ band) emission are correlated on time-scales down to less than 110 s. The shape of the correlation is a power law with index $\gamma$ about 0.2–0.6. The X-ray spectrum is well fitted by a hydrogen neutron star (NS) atmosphere ($kT = 59$–$80$ eV) and a power law (with spectral index $\Gamma = 1.4$–$2.0$), with the spectral shape remaining constant as the flux varies. Both components vary in tandem, with each responsible for about 50 per cent of the total X-ray flux, implying that they are physically linked. We conclude that the X-rays are likely generated by matter accreting down to the NS surface. Moreover, based on the short time-scale of the correlation, we also unambiguously demonstrate that the UV emission cannot be due to either thermal emission from the stream impact point, or a standard optically thick, geometrically thin disc. The spectral energy distribution shows a small UV emitting region, too hot to arise from the accretion disc, that we identified as a hotspot on the companion star. Therefore, the UV emission is most likely produced by reprocessing from the companion star, indeed the vertical size of the disc is small and can only reprocess a marginal fraction of the X-ray emission. We also found the accretion disc in quiescence to likely be UV faint, with a minimal contribution to the whole UV flux.

**Key words:** stars: neutron – X-rays: binaries – X-rays: individual: Cen X-4.

## 1 INTRODUCTION

In low-mass X-ray binaries (LMXBs), a compact object (a neutron star, NS, or a black hole, BH) is accreting matter from a companion star, a main-sequence dwarf, or a white dwarf, or a subgiant with mass smaller (or much smaller) than that of the Sun. Some LMXBs are persistently bright X-ray sources, because they are accreting matter at high rates from their companion star. Their X-ray emission below 10 keV is $L_X \sim 10^{37-38}$ erg s$^{-1}$ (tens of per cent of the Eddington rate), some are persistently not so bright, $L_X = 10^{35}$–$10^{36}$ erg s$^{-1}$, others are instead persistently very faint, $L_X \sim 10^{34-35}$ erg s$^{-1}$, (see e.g. Armas Padilla, Degenaar & Wijnands 2013, and references therein). However, some of them are transient and alternate between long periods of quiescence (lasting up to decades) during which the X-ray emission is faint, generally in the range $L_X = 10^{32}$–$10^{33}$ erg s$^{-1}$, to sporadic periods of intense emission (outbursts, lasting weeks–months or even years), where the X-ray luminosity strongly increases (up to six orders of magnitude at the peak) becoming similar to the persistently bright LMXBs. The physics of LMXBs during their outburst state is thought to

★ E-mail: bernardini@wayne.edu
† Hubble Fellow.

be well established. The general properties of the quiescence to outburst cycle is explained by the disc instability model (DIM; e.g. Cannizzo 1993; Lasota 2001). During outburst, the compact object accretes matter from an accretion disc which has been interpreted has an optically thick and geometrically thin disc (Shakura & Sunyaev 1973) extending close to its surface. On the contrary, the mechanism powering the optical, ultraviolet (UV) and X-ray emission in quiescence is still debated. The emission could be powered by residual accretion, however, the physics of accretion at low Eddington luminosity rates is far from being understood. Several models have been proposed to explain the difference in the emission from an LMXB containing an NS and a BH. However, so far, a unifying scenario which can make a clear prediction, systematically matching the spectral energy distribution (SED), from optical up to the X-ray emission, of both NS and BH quiescent LMXB, is still missing.

Brown, Bildsten & Rutledge (1998) pointed out that the X-ray luminosity of NS LMXB in quiescence should be higher than for BH (deep crustal heating model). Indeed, during an outburst, nuclear reactions are thought to be activated in the upper layers of the NS crust, efficiently transferring energy to the NS core that consequently heats up. Once the crust has thermally relaxed, the energy stored in the core is thermally released on longer time-scales, at a sufficient rate to power the quiescent X-ray emission. This model is best applied to the low quiescent luminosity systems which undergo frequent outbursts. In this model, flux variation (up to a factor of 2–3) only arises between different quiescent epochs due to changes in the composition of the envelope caused by nuclear burning during outburst (Brown, Bildsten & Chang 2002). Immediately after an outburst ends the crust (which has been heated during the outburst) is expected to thermally relax (Rutledge et al. 2002), and such crustal cooling has now been observed in several sources (e.g. Cackett et al. 2008, 2010b, 2013b; Degenaar et al. 2011a; Degenaar, Brown & Wijnands 2011b; Fridriksson et al. 2011, and references therein). The deep crustal heating model does not involve the optical/UV emission at all, and only applies to the thermal X-ray emission from the NS surface. However, in at least some quiescent LMXBs the X-ray flux is variable in a manner that cannot be reconciled with model predictions. Indeed, the thermal X-ray emission in several (though not all) systems seems to be highly variable during quiescence (Campana et al. 1997; Rutledge et al. 2002; Cackett et al. 2010a, 2011), which deep crustal heating alone cannot account for. Moreover, many quiescent NS LMXBs in addition to thermal emission, likely originating from the whole NS surface, also show a power-law spectral component that cannot be explained by this model and whose origin is instead still unclear.

In the mid-1990s a different scenario for quiescent emission, called the advection dominated accretion flow (ADAF), was developed by Narayan & Yi (1995a,b), and consisting in a set of slightly different models. For a review of ADAF models see, for example, Narayan, Mahadevan & Quataert (1998). However, other models, always involving radiatively inefficient accretion flows, were also proposed, like in the case of the adiabatic inflow–outflow solution (ADIOS; Blandford & Begelman 1999, whereby a strong outflow is driven). More particularly, in the ADAF scenario, if the accretion rate drops below a critical value, the standard disc can become unstable and partially evaporate, resulting in a disc truncated further out from the compact object. The matter evaporated from the disc becomes an ADAF, assuming a spherical shape, and rotating much slower than the Keplerian velocity. The characteristic time-scale of accretion is rapid, about 10 per cent of the free fall time-scale, and is faster than the cooling time-scale. This means that the accretion flow becomes radiatively inefficient. The energy released because of viscosity is consequently stored in the accretion flow itself (advection) as entropy (heat) and is not radiated away, unlike the case of a standard disc. Close to the compact object the accretion flow inefficiently cools through synchrotron emission from electrons and ions, producing UV radiation, while further out it is instead the bremsstrahlung which dominates, producing X-ray radiation. In the case of NS LMXBs only, Compton scattering, between the seed photons arising from the NS surface and the hotter electrons in the flow, is the most efficient source of cooling. Finally, if the matter reaches the surface of the NS, all the energy in the flow is transferred to it and then radiated away, while it is lost inside of the event horizon, in the case of a BH. This model predicts brighter X-ray emission from an NS, because its surface is heated by the flow, compared to a BH which instead advects matter and radiation. However, ADAF predictions fit the low quiescent X-ray luminosity of NS LMXB only with the extra action of an efficient propeller effect at the magnetospheric radius which prevents the most part of the accreting matter from reaching the NS surface (see e.g. Asai et al. 1998; Menou et al. 1999a). The development of an ADAF model able to make a clear prediction about NS LMXB O and UV emission is a real challenge. Indeed, the X-ray radiation emitted from the star surface strongly interacts with the accretion flow, which, consequently, cools down because of X-ray inverse Compton scattering. If the Compton cooling is efficient it could be difficult to observe the emission due to the ADAF, because it could become extremely faint (e.g. Menou & McClintock 2001, and references therein).

Another possibility, mainly proposed as an alternative to the ADAF plus propeller model, was developed by Campana & Stella (2000). They suggest that during quiescence the majority (if not all) of the mass transferred from the companion star is accumulated in the outer edge of the accretion disc, while just a tiny fraction of it (if any) is accreted on the compact object. For BH systems, the optical and UV emission is in excess of that emitted by the companion star and gravitationally released in the accretion disc. For NS system instead, the O and UV excess, together with the hard part of the X-ray photons (above 2 keV), are arising from the interaction of a radio pulsar relativistic wind with the matter transferred from the companion, in a region where a shock front takes form. Since the pulsar emission is quenched from the accreting matter, no periodic signal is observed. The whole emission has a power-law spectral shape, extending from the optical to the X-ray band. However, in order to account for the emission of soft X-ray photons (below 2 keV), crustal cooling is needed or, alternatively, the magnetic pole of the NS surface must be hit and heated by relativistic particles moving along the magnetosphere. Variation in the power-law component of NS quiescent LMXBs, would support this model, while variation in the thermal component would favour a scenario involving direct accretion.

Finally, another scenario was proposed to explain the UV emission, which in quiescence is supposed to mainly trace the accretion flow (the companion star is cold, and it is expected to have a minimal contribution at that energy). This involves irradiation and reprocessing of the X-ray emission from the accretion disc (see e.g. van Paradijs & McClintock 1994). However, reprocessing does not explain how X-rays are generated during quiescence. Summarizing, thus far, there is no clear picture of the quiescent accretion flows in LMXB, this is particularly true for that hosting an NS. Indeed, the fact that an NS possesses a surface and a magnetosphere makes it much more complicated than a BH.

Despite much early observational and theoretical work on quiescent LMXBs, there are several crucial questions still remaining

which only simultaneous multiwavelength campaigns can address. For instance, is it accretion at low rates really happening on to NSs, and how exactly does it work? Where precisely does the UV emission arise from? Is the X-ray emission irradiating perhaps the inner edge of the accretion disc, leading to reprocessed UV emission, which would imply that X-ray variability is triggering UV variability? Otherwise, are mass accretion rate fluctuations propagating inwards from the outer disc (UV), up to the NS surface (X-ray), implying that, on the contrary, UV variability is leading the X-ray variability? In order to answer these questions and motivated by recent new evidence for an X-ray–UV correlation in Cen X-4 (Cackett et al. 2013a), we planned a new and unique study of the NS LMXB Cen X-4. Indeed, due to its proximity and the low level of extinction (see Section 2), Cen X-4 is the perfect target for a multiwavelength quiescent study. For the first time ever, we intensively monitored the source on a daily basis, for more than two months, with simultaneous optical, UV and X-ray observation performed by *Swift*.

In Section 2, we report on previous observations of Cen X-4 at which we will later refer in this work. In Section 3, we describe the *Swift* observations and the data reduction. In Section 4, we describe the data analysis and we show the results, that we later discuss in Section 5. In Section 6, we make a summary of the main work conclusions.

## 2 WHAT IS KNOWN ABOUT CEN X-4

Cen X-4 was discovered in 1969 when it entered in an outburst state (Conner, Evans & Belian 1969). 10 year after it experienced a second outburst (Kaluzienski, Holt & Swank 1980) and it has been in quiescence from then on. Moreover, Kuulkers, in't Zand & Lasota (2009) discussed the possibility of the detection of another X-ray burst from Cen X-4 detected by Apollo 15 in 1971. During the decay of the 1979 outburst, an X-ray type I burst was recorded, unambiguously showing that Cen X-4 hosts an NS (Matsuoka et al. 1980). Assuming that during the burst the NS (assuming to have a mass of $1.4\,M_{\odot}$) was emitting at the Eddington limit, an upper limit to its distance was derived and it is 1.2 kpc (Chevalier et al. 1989). The peak of the two outburst luminosity were $\sim 10^{38}$ and $\sim 0.2 \times 10^{38}$ erg s$^{-1}$. Later, González Hernández et al. (2005), from the same burst luminosity, but comparing that with the average peak luminosities of photospheric radius expansion bursts observed in globular clusters, proposed a distance of $1.4 \pm 0.3$ kpc. Note that Kuulkers et al. (2009) also derive an upper limit of 1.2 kpc from their reanalysis of a 1969 X-ray burst from Cen X-4. We assumed a distance of 1.2 kpc since this value matches all these results.

Cen X-4 is one of the most studied LMXB at optical wavelength, since it is the brightest (and nearest) quiescent NS LMXB at this energy. Its mass ratio is well established and results $q = 0.17 \pm 0.06$, while the masses of the NS and that of the companion are constrained to lie within $0.49 < M_{\rm NS} < 2.49$ and $0.04 < M_{\rm c} < 0.58$ (Torres et al. 2002). This implies, assuming that the secondary fills its Roche lobe, that the companion stellar radius is $0.5 < R_{\rm c}/R_{\odot} < 1.2$ (González Hernández et al. 2005). The companion star is an evolved main-sequence star of the K3–7 V type (Chevalier et al. 1989; D'Avanzo et al. 2005) with an effective temperature $T_{\rm eff} = 4500 \pm 100$ K (González Hernández et al. 2005). Photometric optical measure showed that its luminosity is modulated at a period of 15.1 h, which has been interpreted as the orbital period. The modulation in the *V* bands has an amplitude of 0.2 mag, which corresponds to a flux variation of about 17 per cent. The accretion disc, which has an inclination of 30°–46°, is bright at optical wavelengths, producing ∼25 per cent of the total light in the *V* band (Chevalier et al. 1989), while its contribution in the infrared (IR) is lower, about 10 per cent (Shahbaz, Naylor & Charles 1993). By knowing the orbital period and the mass ratio, and assuming an NS of $1.4\,M_{\odot}$, we derived some of the orbital parameters that we will refer to later: the orbital separation $a$ between the two stars of the binary is $\sim 2.5 \times 10^{11}$ cm, the distance from the centre of the companion and the inner Lagrangian point $b_1$ is $\sim 1.7 \times 10^{11}$ cm, the outer disc radius is $\sim 1.5 \times 10^{11}$ cm (Frank, King & Raine 2002).

During quiescence, the spectrum of Cen X-4 is well fitted by a two component model made by a power law, with spectral index $\alpha \sim 1.4$–$1.8$, plus an NS atmosphere made of pure hydrogen of effective temperature $kT_{\rm eff} = 50-70$ eV, multiplied by a low level of interstellar absorption $N_{\rm H} = 4.9 \times 10^{20}$ cm$^{-2}$ (Cackett et al. 2013a). The X-ray light curve of Cen X-4 during quiescence is highly variable on a wide range of time-scales, from hundreds of seconds to years, with count rate variations up to a factor of 3 in only 4 d. The 0.5–10 keV quiescent luminosity was found to be $\sim 0.76$–$4.91 \times 10^{32}$ erg s$^{-1}$ (Campana et al. 1997, 2004; Rutledge et al. 2001; Cackett et al. 2010a, 2013a).

## 3 OBSERVATIONS AND DATA REDUCTION

The *Swift* satellite has on board three telescopes covering, respectively, the optical/*UV* band, Ultraviolet/Optical Telescope (UVOT; Roming et al. 2005; Breeveld et al. 2010), the X-ray Telescope, XRT, and the $\gamma$-ray band, Burst Alert Telescope, (BAT; Gehrels et al. 2004). Because of the soft nature of the X-ray emission from Cen X-4, we only analysed data from the XRT, covering the 0.3–10 keV energy range, while the source is undetected in the BAT range. Concerning the optical/UV analysis we explored data in two optical filters, *V* (5468 Å) and *B* (4392 Å) and four *UV* filters *U* (3465 Å), *UVW*1 (2600 Å), *UVM*2 (2246 Å) and *UVW*2 (1928 Å).

*Swift* observed Cen X-4 for a total of 62 times[1] (60 times in PC mode), 58 of these pointings are performed on a daily basis between 2012 June 5 and August 8. The 60 observations in PC mode that we used were performed in the following way: one 5 ks pointing was followed by four pointings of 1 ks each and so on. The UVOT configuration was set as follows: for the observations lasting 5 ks the *UVW*2, *UVM*2, *UVW*1, *U*, *B* and *V* filters are sequentially used, while for the observation lasting 1 ks, only the *UVW*1 and *V* filters are used. Each observation made by *Swift* is always composed of multiple snapshots, both in the case of XRT and UVOT, the total number of which is variable among different observations. For each single XRT snapshot, multiple UVOT (sub)snapshots are made, one for each of the six available bands (*UVW*2, *UVM*2, *UVW*1, *U*, *B* and *V*) in case of 5 ks observation, while one for the *UVW*1 and one for the *V* band, in case of 1 ks observation. We first analysed the average data of each single observation, summing together all the XRT snapshots and all the (sub)snapshots of the same UVOT filter. Consequently, each point in the X-ray light curve has an exposure time of 1–5 ks, while each pointing in the O–UV light curve lasts from few hundred seconds up to about 2 ks. Secondly, we separately analysed the data of all single UVOT (sub)snapshot, then extracting only the part of the XRT snapshot exactly simultaneous to the UVOT one. This procedure results in single exposures ranging from about few tens of seconds up to about 2 ks.

[1] The observation id number goes from 00035324001 to 00035324065 with the exception of 00035324037/49/64.

### 3.1 XRT data reduction

In order to perform an accurate data analysis of the source variability with *Swift* data, it is mandatory to remove the contamination from bad pixels and bad columns which is affecting the XRT CCD after it was hit by a micrometeorite in 2005. We followed the detailed online thread procedure available at http://www.swift.ac.uk/analysis/xrt/xrtpipeline.php, that we summarize below.

Using the HEASOFT version 6.12[2] we first produced the cleaned event files of each of the 60 single pointings in PC mode with the *xrtpipeline* command by also creating the pointing exposure map, manually providing the best source position. Using the cleaned event file, we produced the source image and then extracted the source spectrum from a circular region of 20 pixel size, centred at the source position. The background spectrum was extracted in a clean region of the sky near the source, from a region of 80 pixel size. Due to the low source X-ray flux ($\sim$0.006–0.021 c s$^{-1}$), no pile-up correction is needed in the extraction of the source spectrum. The ancillary response file (ARF) was then created, referring to the exposure map previously generated, by using the *xrtmkarf* tool, with the point spread function correction active which, among other things, ensures a correction for hot columns and bad pixels.

We also produced the cleaned event file for each XRT snapshot of each observation and, on a shorter time-scale, also for all the multiple subintervals, lasting a few hundred seconds on average, corresponding to the time interval of effective UVOT snapshot exposure. In order to extract the source spectrum for each time interval of interest, we followed the procedure described above, producing a single exposure map for each of the time intervals. Finally, we calculated the source background-subtracted count rate from the spectral files taking into account the ratio between the area of the source region and background region.

In order to create spectra with the maximum possible signal-to-noise ratio (S/N) we also summed together spectra from different XRT pointing, with comparable count rate, using the following procedure. We first sum all the individual event files of interest by using *XSelect*, then we summed, one by one, the individual exposure maps using the command *sum ima* in the XIMAGE package. We finally extracted the summed spectrum with *XSelect* and generated the summed ARF file using the summed exposure maps. Before fitting, the summed spectra were rebinned in order to have, at least, 20 counts per bin, and fits are performed using the $\chi^2$ statistic. All spectral fits are made with XSPEC version 12.7.1 (Arnaud 1996), and the latest calibration files available in 2012 October.

### 3.2 UVOT data reduction

We applied the following procedure consisting of five consecutive steps (each one using a specific tool) to each observation and each band filter contained in it. The five steps are (1) *uvotbadpix*, (2) *uvotexpmap*, (3) *uvotimsum*, (4) *uvotdetect* and (5) *uvotsource*.

In more detail, starting from the raw image file, we first produced the bad pixel map with the *uvotbadpix* tool. As a second step, from the level II image fits file, we created the exposure maps, by using the bad pixel map previously generated as reference for bad pixels positions, and the *uat.fits* file as attitude file (more accurate than the *sat.fits* file). We summed all the multiple image extensions contained in the level II image fits file, producing the total image, by using the *uvotimsum* tool. We did the same for the exposure map, by using the *uvotimsum* tool we built the total exposure map. We run the *uvotdetect* tool to detect all the source in the summed image above a 3$\sigma$ threshold. We identified the closest source to the Cen X-4 coordinates in the output *uvotdetect* list file, also checking that the source was always detected. Finally, we extracted the background-subtracted source count rate by using the *uvotsource* tool, after defining the source and the background regions with a circle of 5 and 10 arcsec size, respectively. The source region is centred at the best position known for Cen X-4, while the background region is taken from a close by region, not contaminated by other sources.

We extracted the source count rate for each single snapshot, of each band, for all the pointings, following the same procedure described above, except for the fact that the exposure maps and the image files were not summed together (step 3 of the total reduction procedure was skipped as in this case we are only looking at individual exposures).

[2] http://heasarc.gsfc.nasa.gov/lheasoft/

## 4 ANALYSIS AND RESULTS

### 4.1 Multiwavelength light curve

We first analysed the background-subtracted light curves in all the energy bands. The source is highly variable in all bands. Particularly interesting is the comparison between the X-ray and the *UVW*1 and *V* bands, the three energy intervals for which the most pointings (60) are accumulated. Indeed, due to the selected observing strategy, *Swift* was always observing in those bands. We show the light curves in Fig. 1. For plotting purposes, we do not show the two first pointings ($t = -2066.8$ d and 0, where $t = 0$ is 2012-05-01 07:47:32.44 UTC) that do not belong to the main observational campaign. The X-ray and *UVW*1 light curve seem to follow roughly the same pattern, showing both long-term (months) and short-term (days) variability. They both show randomly distributed peaks in the count rate at the same time. The *V* light curve is much less variable, however, the uncertainties here are larger. We note that the recorded peaks are independent from the orbital period which is only $\sim$15.1 h (Chevalier et al. 1989). Zurita, Casares & Shahbaz (2002) also measured flare-like optical variability from Cen X-4 showing that it is independent from the orbital period.

We calculated the fractional root-mean-square variability ($F_{\rm var}$) for the light curves in Fig. 1 (see Vaughan et al. 2005 for more details about $F_{\rm var}$). All uncertainties are hereafter at the 1$\sigma$ confidence level. $F_{\rm var}$ is 73.0 $\pm$ 1.5 per cent for the X-ray band, 50.0 $\pm$ 1.4 per cent for the *UVW*1 band and 10.0 $\pm$ 1.6 per cent for the *V* band, implying that the X-ray emission is the most variable. The most significant changes in the X-ray count rate are detected between 39.5 and 43.3 d and between 97.2 and 101.5 d, where the count rate, respectively, decreases by a factor of $\sim$13 and increases by a factor of $\sim$22 in 4 d only (from 0.21 $\pm$ 0.01 to 0.016 $\pm$ 0.04 c s$^{-1}$ and from 0.006 $\pm$ 0.003 to 0.13 $\pm$ 0.01 c s$^{-1}$, respectively). In the same time window, the *UVW*1 emission is changing less, and decreases by a factor of $\sim$5 (from 0.70 $\pm$ 0.04 to 0.13 $\pm$ 0.03 c s$^{-1}$) and increases by a factor of $\sim$14 (from 0.04 $\pm$ 0.03 to 0.55 $\pm$ 0.04 c s$^{-1}$), respectively.

### 4.2 Structure function

The first-order structure function is commonly used to establish the time-scale and the intrinsic variability in the light curve of active galactic nucleus (see e.g. Do et al. 2009, and references therein). The structure function is related to the autocorrelation function and the power spectrum and is an alternative way of determining the power at a given time-scale. In our case, we have a light curve

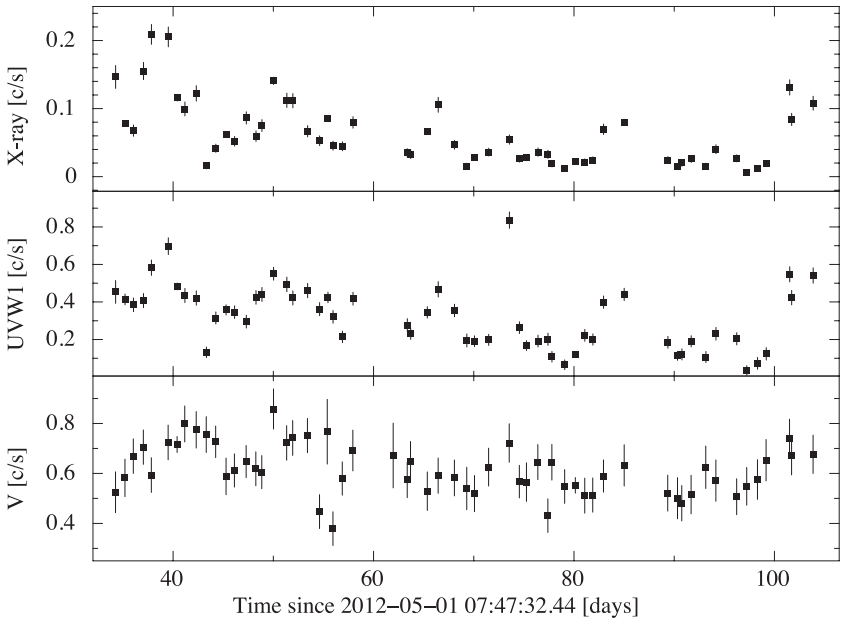


**Figure 1.** Light curves for Cen X-4 in three different energy ranges. 0.3–10 keV, X-ray (top), *UVW*1, 2600 Å (centre) and *V*, 5468 Å (bottom). For plotting purposes, we selected the reference time as 2012-05-01 07:47:32.44 UTC, which corresponds to the second *Swift* pointing. The only two pointings which are not plotted here correspond to $t = 0$ d and $-2066.8$ d.

that is not evenly sampled, thus determining the power spectrum becomes complicated. The structure function provides us with a straightforward method in the time domain.

Here, we used (for the very first time) the structure function to define the quiescent variability of Cen X-4. We compute the structure function for the three light curves (X-ray, *UVW*1 and *V*) in Fig. 1. The structure functions are computed after having normalized the light curves to their average values (this allows for a direct comparison of the intensity of the variability among the three light curves). For this structure function analysis, we also included the point at $t = 0$ in the light curve (not shown in Fig. 1), so the light curve covers a total of ∼104 d. The first-order structure function is here defined as

$$V(\tau) = \langle [s(t+\tau) - s(t)]^2 \rangle, \quad (1)$$

where the bracket denotes an average quantity and $s(t)$ is a set of measures (the count rate in each band) performed at the time $t$. Since our data are unevenly sampled, we measured $[s(t+\tau) - s(t)]^2$ for all the existing couples of time lags. Then we binned the time lags, with a variable bin size in order to have a comparable number of points in each bin with a minimum number of points equal to 40. The centre of each bin is the time lag for that bin, while the average of $V(\tau)$ is the value of the structure function for each bin at that time lag. The error associated with each bin is the standard deviation of the structure function $V(\tau)$ divided by the square root of the number of points in the bin ($\sigma_{\rm bin}/\sqrt{N_{\rm bin}}$). The three structure functions are showed in Fig. 2. The shape of an ideal structure function is expected to follow a shape consisting of two plateaus, the first one at the time-scale of the noise and the second at a time-scale longer than the inspected physical process, connected to each other by a power law which provides a measure of the time-scale of the variability (see, e.g. Hughes, Aller & Aller 1992, for a clear description and example). The slope of the structure function is related to the slope of the power spectrum. For instance, a power spectrum with $P(f) \propto f^{-2}$ will show a first-order structure function where $V(\tau) \propto \tau^1$ (e.g. Hughes et al. 1992). We find the power-law index of the structure

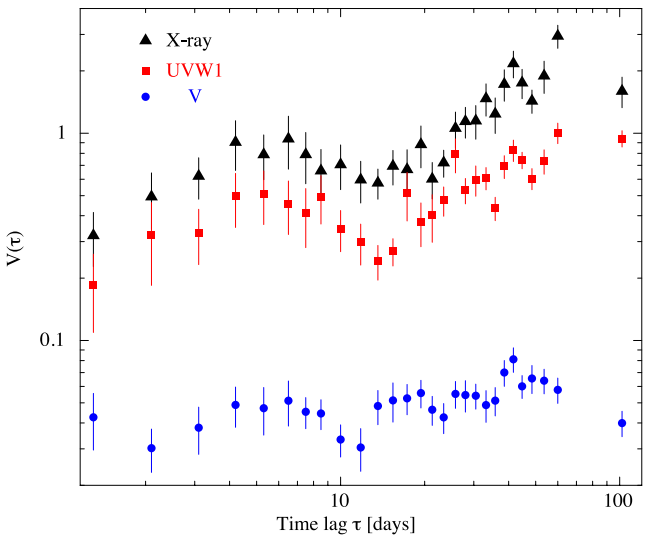


**Figure 2.** First-order structure function $V(\tau)$ as a function of the time lag for the three light curves (X-ray, *UVW*1 and *V*) in Fig. 1. The light curves have been normalized to their average value before computing the structure function. This allows for easy comparison of the variability amplitude in each band.

function of Cen X-4 to be $1.0 \pm 0.1$ and $0.8 \pm 0.1$ and $0.3 \pm 0.1$ in the case of the X-ray, *UVW*1 and *V*, respectively, for $11 < \tau < 60$. The fit was performed in the time lag range of 11–60 d (where the power law extends) and gives $\chi^2_\nu = 1.36$, 1.70 and 0.86 (16 d.o.f.), respectively. The slope of the X-ray and *UVW*1 band is consistent with a power spectrum with index $-2$ (red noise also known as random walk noise) as typically seen in accreting systems, while the slope of the *V* band is different and, consequently, it may be associated with another underlying process. The structure function also shows that the amplitude of the variability is greater in the X-ray band than in others, and the *UVW*1 amplitude is greater than

in the *V* band (matching the results of the $F_{\rm var}$ analysis). The time-scale of the variability goes from 10 d up to at least 60 d (there is only one point in the light curve a longer time-scale). However, an excess is present at about 4 to 5 d. This is likely linked to the rise and decay time of the peaks in the light curve. So, variability is also detected at this time-scale.

### 4.3 Long time-scale correlation

We studied the correlation between the X-ray count rate and that of all *UV* and optical bands on a time-scale corresponding to the XRT exposure, $t = 1$–$5$ ks ($t \leq 5$ ks hereafter). This means to compare the average count rate of each XRT pointing with that of the simultaneous *O* and *UV* bands summed snapshots (see Fig. 3). In order to prove if a correlation is present, we first fit the data with a constant, then with a constant plus a linear ($y = y_0 + ax$) and with a constant plus a power law ($y = y_0 + ax^{\gamma}$). We verified the statistical significance of the inclusion of the linear and the power-law component with respect to a constant with an *F*-test. If they are significant at more than the $3\sigma$ confidence level, we consider that a correlation exists. Then, we verified if the shape of the correlation is a linear or a power-law function. Since we are comparing two different models, with a different number of d.o.f., we cannot use an *F*-test. Consequently, we applied the following procedure: we compared the constant plus linear fit with that of a constant plus power law, by estimating the $\chi^2$ distance, here defined as $x$, from its expectation value in unit of $\sigma_{\chi^2}$. Since $\sigma^2_{\chi^2} = 2$ d.o.f. $\Rightarrow \sigma_{\chi^2} = \sqrt{2\text{d.o.f.}}$, and so $\frac{(\chi^2 - \text{d.o.f.})}{\sigma_{\chi^2}} = x[\sigma_{\chi^2}]$, where d.o.f. are the degrees of freedom. We consider as the most likely shape of the correlation that having the lower value of $x$. All fit results are reported in Table 1. Note that for the *UVW*1 band, we excluded from the correlation study the anomalously high count rate ($\sim 0.85\,\mathrm{c\,s^{-1}}$) point at $t = 75.5$ d

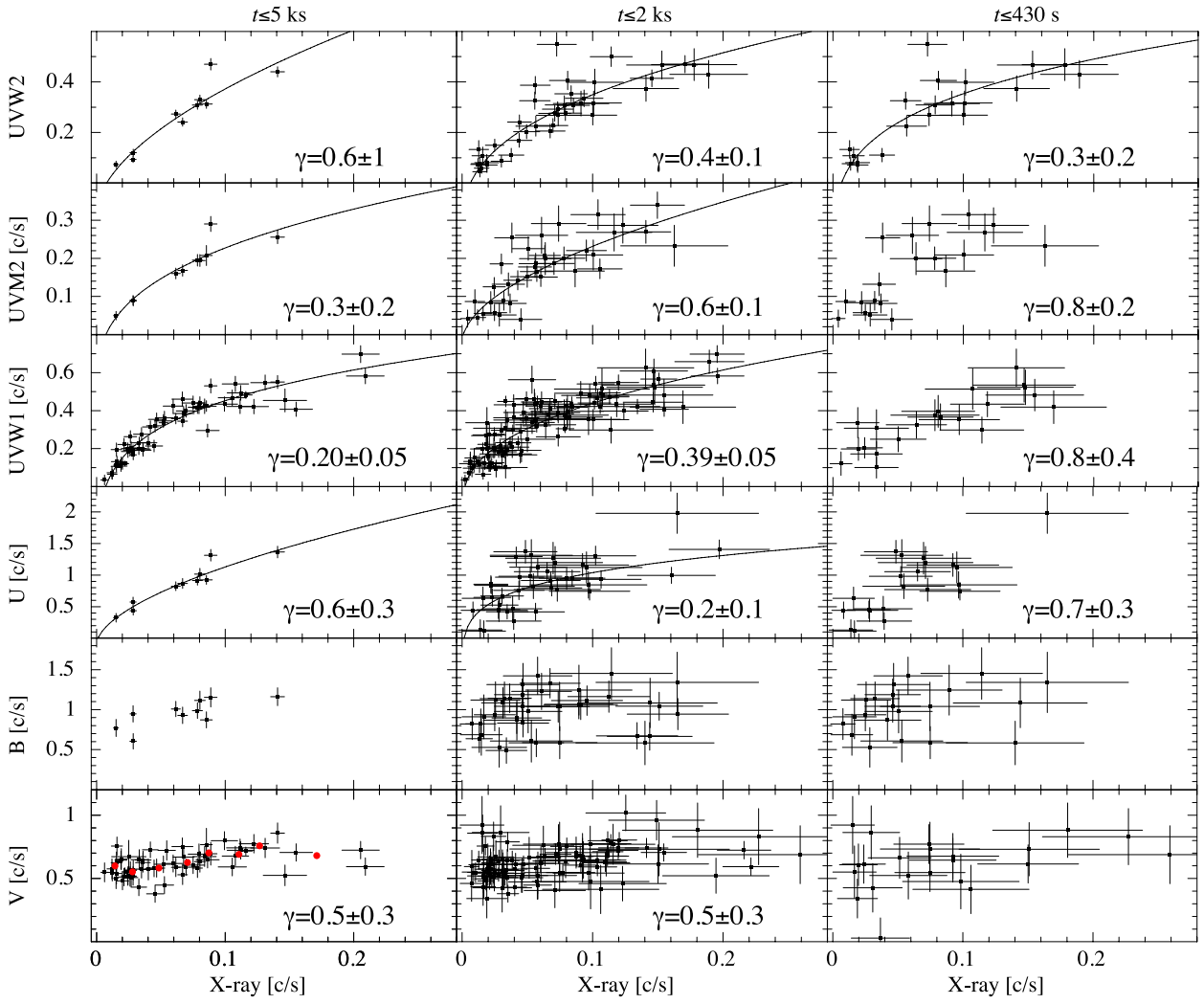


**Figure 3.** Study of the X-ray versus UV–O correlation as a function of the energy interval and the time-scale. Energy increases from bottom to top, while the time-scale decreases from left to right. The solid line represents the best-fitting model, a constant plus a power law, which is plotted only when it is unambiguously determined. The value of the slope $\gamma$ for the constant plus power-law model is also reported in the lower-right part of each panel. A correlation is always found, exception are the *B* band (all time-scale), where, however, no high X-ray count rate coverage is available, and the *V* band (only in the case of $t \leq 110$ s), likely because of the limited number of points. Left: X-ray versus UV–O average count rates on the XRT pointing time-scale ($t \leq 5$ ks). For plotting purposes, the *V* band count rate is also averaged (red circles) in eight X-ray count rate subintervals (0–0.002, 0.002–0.004, 0.004–0.006, 0.006–0.008, 0.008–0.010, 0.010–0.012, 0.012–0.022 $\mathrm{c\,s^{-1}}$). Center: X-ray versus UV–O count rate on the UVOT snapshot time-scale ($t \leq 2$ ks). Right: X-ray versus UV–O count rate on the UVOT shorter snapshot time-scale $t \leq 430$ s (here the exact time-scale depends on the energy interval. See the text for more details).

**Table 1.** Study of the correlation between X-ray and *UV* and *O* bands on the time-scale of an XRT observation, $t \leq 5$ ks. The results of the fit with a linear (co+li) and a power law (co+pow) are reported only when these components are statistically significant. *Co*, *Li*, $\gamma$ and *a* are the values of the constant, the slope of the linear and the index of the power law with its multiplicative coefficient *a*, respectively, while $\rho$ is Spearman's coefficient and *P* the null hypothesis probability (no correlation). Uncertainties are $1\sigma$ confidence level.

| Band | Model | *Co* | *Li* | $\gamma$ | *a* | $\chi^2_\nu$/d.o.f. | Sign. $\sigma$ | $x$ $\sigma_{\chi^2}$ | $\rho$ | *P* |
|---|---|---|---|---|---|---|---|---|---|---|
| *UVW*2 | co | 0.22 ± 0.05 | | | | 69.7/9 | | 145.8 | | |
| – | co+li | 0.02 ± 0.01 | 3.5 ± 0.1 | | | 7.9/8 | 4.0 | 13.9 | 0.964 | $7.3 \times 10^{-6}$ |
| – | co+pow | −0.11 ± 0.06 | | 0.6 ± 0.1 | 1.8 ± 0.3 | 7.3/7 | 3.6 | 11.7 | | |
| *UVM*2 | co | 0.14 ± 0.05 | | | | 25.9/9 | | 52.9 | | |
| – | co+li | 0.04 ± 0.01 | 1.9 ± 0.1 | | | 3.6/8 | 3.8 | 5.2 | 0.964 | $7.3 \times 10^{-6}$ |
| – | co+pow | −0.2 ± 0.1 | | 0.3 ± 0.2 | 0.8 ± 0.1 | 2.6/7 | 3.7 | 2.9 | | |
| *UVW*1 | co | 0.284 ± 0.004 | | | | 25.1/58 | | 129.6 | | |
| – | co+li | 0.109 ± 0.006 | 3.3 ± 0.1 | | | 5.0/57 | >8 | 21.1 | 0.934 | $3.6 \times 10^{-27}$ |
| – | co+pow | −0.7 ± 0.3 | | 0.20 ± 0.05 | 1.8 ± 0.3 | 2.3/56 | >8 | 7.0 | | |
| *U* | co | 0.80 ± 0.02 | | | | 18.2/9 | | 36.5 | | |
| – | co+li | 0.25 ± 0.04 | 9 ± 1 | | | 2.0/8 | 4.1 | 1.9 | 0.976 | $1.5 \times 10^{-6}$ |
| – | co+pow | −0.1 ± 0.3 | | 0.6 ± 0.3 | 5 ± 2 | 1.8/7 | 3.6 | 1.6 | | |
| *B* | co | 0.94 ± 0.3 | | | | 2.8/9 | | 3.8 | | |
| – | co+li | | | | | 1.4/8 | 2.2 | | 0.697 | 0.025 |
| – | co+pow | | | | | 1.6/7 | 1.6 | | | |
| *V* | co | 0.61 ± 0.01 | | | | 2.0/59 | | 5.3 | | |
| – | co+li | 0.55 ± 0.02 | 1.1 ± 0.2 | | | 1.4/58 | 4.4 | 2.2 | 0.554 | $4.3 \times 10^{-6}$ |
| – | co+pow | 0.5 ± 0.2 | | 0.5 ± 0.3 | 0.6 ± 0.3 | 1.4/57 | 4.2 | 2.1 | | |

(obsid 00035324038), since it evidently lies significantly outside of the correlation. Moreover, for that observation no coverage is provided in the other *UV* bands, and so it is not possible to cross-check if such high count rate is also present in there. We note that optical flares not associated with the X-ray source, but likely linked to some mechanism in the companion star or in the disc, have been already observed from Cen X-4 (Zurita et al. 2002).

We always found a correlation between X-ray and all the *UV* bands (*UVW*2, *UVM*2, *UVW*1 and *U*), see Fig. 3. Although some scatter is always present, the fit with a constant plus a power law is always preferred in terms of *x*. The significance for the inclusion of a power law in the fit ranges from $3.6\sigma$ up to more than $8\sigma$ in the case of the *UVW*1, where more data points are available. The value of the power-law index $\gamma$ ranges from 0.20 ± 0.05 (*UVW*1) to 0.6 ± 0.3 (*U*). No correlation is detected in the case of the optical *B* band (the significance for the inclusion of a power law is only $1.6\sigma$, see also Table 1). However, here, only nine points are available, moreover, none of them is covering the high count rate region above 0.17 c s$^{-1}$, where a power law and a linear function clearly reveal their difference. A correlation with the *V* band is also found. Either a power law or a linear function, both significant at more than $4\sigma$, provide comparable fit in terms of *x*.

Note that Cackett et al. (2013a) found a linear correlation between the X-ray and the UV (*UVW*1 *XMM–Newton* band) in Cen X-4, while we find here a power law to be the best-fitting shape of the correlation. This can be easily explained by the fact that we have a significantly higher number of data points and, consequently, we are covering a wider dynamic range in X-ray count rate, especially at high X-ray count rate (e.g. above 0.17 c s$^{-1}$), where a linear function and a power law really show their difference in shape.

### 4.4 Short and very short time-scale correlation

In order to further explore the presence and the nature of a correlation between X-ray and all *UV–O* bands emission, we compared the count rates on shorter time-scale. We selected that of the single UVOT snapshot inside of a *Swift* observation, where *t* is going from ∼10 s up to ∼2 ks, so the explored time-scale here is $t \leq 2$ ks. In this case, a higher number of data points is available, ranging from ∼40 up to ∼110, depending on the band (see Fig. 3). Finally, we investigate the correlation on the shortest time-scale available by selecting the shortest UVOT snapshot only, with the condition to maintain a statistically relevant number of data points ($n \geq 20$). The correlation on such short time-scales was never studied before.

Using the above conditions, we explored, for the different bands, the following time-scale: $t \leq 430$ s for *UVW*2, $t \leq 320$ s for *UVM*2, $t \leq 150$ s for *UVW*1, $t \leq 110$ s for *U*, $t \leq 110$ s for *B* and $t \leq 110$ s for *V*. Consequently, we define the very short time-scale as $t \leq 430$ s. Although, once again, some scatter is always present, as in the case of $t \leq 5$ ks, a correlation between the X-ray and all *UV* bands is always found, for both $t \leq 2$ ks and ≤430 s. This is the very first time that a correlation is observed at that time-scale. In the case of $t \leq 2$ ks (see Table 2), the most likely shape of the correlation is always a power law, as *x* is always lower than in the case of the fit with a linear function. The significance of the inclusion of the power-law function with respect to a constant is always greater than $4\sigma$. We found $\gamma$ ranging from 0.2 ± 0.1 in the case of *U* band up to 0.6 ± 0.1 for the *UVM*2 band. No correlation is detected with the *B* band, while a correlation is found with the *V* band, where both a linear and a power-law shape are equally acceptable from a statistical point of view. In the case of $t \leq 430$ s (see Table 3), for the *UVW*2 band, the most likely shape of the correlation is a power law ($\gamma = 0.3 \pm 0.2$), while it could be either a power law or a linear for the *UVM*2, *UVW*1 and *U* bands. However, we note that in the latter bands, due to the limited number of data points, the explored X-ray count rate is always lower than 0.17 c s$^{-1}$. No correlation is detected either with the *B* or the *V* band (likely because of the limited number of data points and because the high X-ray count rate is not covered).

Summarizing, we studied the presence of a correlation between the X-ray count rate and that of *UV* and optical bands (six in total) for three time-scales ($t \leq 5$, ≤2 ks, ≤430 s). We found a statistically significant correlation in 14 cases over a total of 18 (the exceptions are the *B* band, for all time-scale, and the *V* band, for the very short

**Table 2.** Study of the correlation between X-ray and *UV–O* bands for the time-scale of an UVOT snapshot, $t \leq 2$ ks. See Table 1 for the definitions of the parameters reported here.

| Band | Model | *Co* | *Li* | $\gamma$ | *a* | $\chi^2_\nu$/d.o.f. | Sign. $\sigma$ | $x$ $\sigma_{\chi^2}$ | $\rho$ | *P* |
|---|---|---|---|---|---|---|---|---|---|---|
| *UVW2* | co | 0.217 ± 0.005 | | | | 18.1/39 | | 75.7 | | |
| – | co+li | 0.056 ± 0.008 | 2.8 ± 0.1 | | | 4.1/38 | >8 | 13.6 | 0.876 | $1.4 \times 10^{-13}$ |
| – | co+pow | −0.18 ± 0.08 | | 0.4 ± 0.1 | 1.3 ± 0.1 | 3.3/37 | >8 | 9.8 | | |
| *UVM2* | co | 0.144 ± 0.005 | | | | 7.7/36 | | 28.3 | | |
| – | co+li | 0.051 ± 0.08 | 1.8 ± 0.1 | | | 2.5/35 | >8 | 6.4 | 0.817 | $6.9 \times 10^{-10}$ |
| – | co+pow | −0.02 ± 0.05 | | 0.6 ± 0.1 | 0.9 ± 0.2 | 2.4/34 | >8 | 5.7 | | |
| *UVW1* | co | 0.283 ± 0.004 | | | | 14.6/108 | | 99.6 | | |
| – | co+li | 0.125 ± 0.006 | 3.0 ± 0.1 | | | 4.3/107 | >8 | 24.2 | 0.849 | $2.0 \times 10^{-31}$ |
| – | co+pow | −0.12 ± 0.05 | | 0.39 ± 0.05 | 1.38 ± 0.06 | 3.4/106 | >8 | 17.5 | | |
| *U* | co | 0.79 ± 0.02 | | | | 4.9/39 | | 17.3 | | |
| – | co+li | 0.50 ± 0.04 | 5.0 ± 0.6 | | | 3.1/38 | 4.1 | 9.3 | 0.648 | $6.5 \times 10^{-6}$ |
| – | co+pow | −0.8 ± 0.1 | | 0.2 ± 0.1 | 2.9 ± 0.2 | 3.0/37 | 4.0 | 8.5 | | |
| *B* | co | 0.94 ± 0.03 | | | | 1.5/39 | | 2.1 | | |
| – | co+li | | | | | 1.5/38 | <0.5 | 2.2 | 0.262 | 0.103 |
| – | co+pow | | | | | 1.5/37 | <0.5 | 2.2 | | |
| *V* | co | 0.62 ± 0.01 | | | | 1.6/102 | | 4.5 | | |
| – | co+li | 0.55 ± 0.02 | 1.0 ± 0.2 | | | 1.3/101 | 4.6 | 2.3 | 0.391 | $4.8 \times 10^{-5}$ |
| – | co+pow | 0.5 ± 0.2 | | 0.5 ± 0.3 | 0.6 ± 0.3 | 1.3/100 | 4.3 | 2.3 | | |

**Table 3.** Study of the correlation between X-ray and *UV* and *O* bands for the shortest UV snapshot only. Here, the explored time-scale depends on the energy interval and it is consequently reported for each band. See Table 1 for the definitions of the parameters reported here.

| Time-scale (s) | Band | Model | *Co* | *Li* | $\gamma$ | *a* | $\chi^2_\nu$/d.o.f. | Sign. $\sigma$ | $x$ $\sigma_{\chi^2}$ | $\rho$ | *P* |
|---|---|---|---|---|---|---|---|---|---|---|---|
| 430 | *UVW2* | co | 0.23 ± 0.01 | | | | 14.6/19 | | 42.0 | | |
| | – | co+li | 0.07 ± 0.02 | 2.6 ± 0.2 | | | 4.7/18 | 4.4 | 11.1 | 0.789 | $3.5 \times 10^{-5}$ |
| | – | co+pow | −0.4 ± 0.3 | | 0.3 ± 0.2 | $1.3 \pm ^{1}_{0.1}$ | 3.8/17 | 3.7 | 8.3 | | |
| 320 | *UVM2* | co | 0.13 ± 0.1 | | | | 7.7/20 | | 20.0 | | |
| | – | co+li | 0.05 ± 0.02 | 2.0 ± 0.2 | | | 2.8/18 | 3.7 | 5.4 | 0.759 | 0.0001 |
| | – | co+pow | 0.02 ± 0.03 | | 0.8 ± 0.2 | 1.4 ± 0.7 | 2.6/17 | 3.6 | 5.6 | | |
| 150 | *UVW1* | co | 0.31 ± 0.02 | | | | 3.7/20 | | 8.5 | | |
| | – | co+li | 0.14 ± 0.03 | 2.4 ± 0.3 | | | 1.1/19 | 4.8 | 0.2 | 0.813 | $7.5 \times 10^{-6}$ |
| | – | co+pow | 0.10 ± 0.07 | | 0.8 ± 0.4 | 2 ± 1 | 1.1/18 | 4.3 | 0.3 | | |
| 110 | *U* | co | 0.71 ± 0.04 | | | | 5.5/20 | | 14.1 | | |
| | – | co+li | 0.26 ± 0.07 | 9 ± 1 | | | 2.8/19 | 3.4 | 5.7 | 0.668 | 0.0009 |
| | – | co+pow | 0.1 ± 0.4 | | 0.7 ± 0.3 | 5 ± 3 | 2.9/18 | 3.0 | 5.8 | | |
| 110 | *B* | co | 0.97 ± 0.05 | | | | 1.4/20 | | 0.8 | | |
| | – | co+li | | | | | 1.3/19 | <0.5 | 0.7 | 0.347 | 0.1236 |
| | – | co+pow | | | | | 1.3/18 | <0.5 | 0.9 | | |
| 110 | *V* | co | 0.59 ± 0.04 | | | | 1.3/21 | | 0.9 | | |
| | – | co+li | | | | | 1.2/20 | 1.2 | 0.6 | 0.238 | 0.2864 |
| | – | co+pow | | | | | 1.2/19 | 0.5 | 0.5 | | |

time-scale only). In nine cases over a total of 14 where a correlation is significant, its most likely shape is a power law. A linear shape is instead disfavoured (see Fig. 3 and see the value of $x$ in Tables 1–3). Finally, we cross-checked the results of the above correlation study, for all time-scale, with a Spearman's correlation test. We reported in Tables 1–3 the value of Spearman's coefficient $\rho$ and the null hypothesis probability (*P*), which is the probability that any random sample of uncorrelated experimental data points, of an uncorrelated parent population, would yield a Spearman's coefficient value equal to $\rho$. The results of Spearman's test fully confirm our first results. There is always a strong correlation between the X-ray and UV emission in all bands for all time-scale, a less intense but still statistically significant correlation is also found with the optical *V* band emission (for $t \leq 5$ and $\leq 2$ ks). No statistically significant correlation is detected with the *V* band for $t \leq 110$ s and with the *B* band (all time-scale), very likely because of the limited number of data points (indeed the probability *P* is strongly dependent on the number of data points).

### 4.5 X-ray spectral analysis

As a first step we verified that the average spectral shape is not clearly changing among different pointings with comparable count rate. We visually inspected the spectral shape of each pointing, then we fitted the spectra with a simple model consisting of a power law multiplied by the Galactic photoelectric absorption *phabs*. We imposed *phabs* to be constant between observations and we left the power law free to vary. The power-law photon index was constant within statistical uncertainty, while only the normalization (flux) was found to change. We concluded that the spectral shape is roughly constant among different pointings with comparable count rate. Then, in order to inspect possible spectral change as a

function of the flux (count rate), we selected three count rate range: low $<0.07\,\mathrm{c\,s^{-1}}$, medium 0.07–0.11 $\mathrm{c\,s^{-1}}$ and high $>0.11\,\mathrm{c\,s^{-1}}$ (see Fig. 1), and we produced three summed spectra. This choice allowed us to maintain a comparable number of count among the three spectra. The low state spectrum has ∼2100 counts for 67 ks of exposure, the medium state spectrum ∼2300 counts for 30 ks and the high state ∼1400 counts for 11.5 ks.

We selected a model made by the sum of an NS atmosphere composed of pure hydrogen *nstamos* (Heinke et al. 2006), where the magnetic field is assumed negligible (less than $10^9$ G), plus a power law, both multiplied by *phabs*, which accounts for photoelectric absorption due to the interstellar medium. We note that the use of the *nstamos* model is not formally correct if the source is still accreting also at low Eddington luminosity rates. This is a scenario that we want to test in the following for Cen X-4. Zampieri et al. (1995) developed a model called *zamps*, explicitly to reproduce the thermal emission from a non-magnetized NS, accreting at low rates ($10^{-7} \lesssim L/L_{\rm Edd} \lesssim 10^{-3}$). However, Zampieri et al. (1995) and Soria et al. (2011) showed that the fits performed with the *zamps* model and that with the *nsa* model, describing an NS with hydrogen atmosphere, are virtually identical for the level of S/N of our data. Consequently, to enable comparison with previous work, we decided to use the *nstamos* model.

Previous analysis showed that both the thermal component and the power-law component must vary. In the case of the thermal component, either the radius or the temperature can change, providing equally acceptable fits. Here, we decided to first fix the NS radius at 10 km, initially imposing that all the surface is emitting (normalization fixed to one). We fixed the source distance to 1.2 kpc assuming an NS mass of 1.4 $\mathrm{M_\odot}$. We fitted the three spectra together.

We first verified that the spectral changes among the three different count rate spectra, high (h), medium (m), low (l), cannot be due to a change in the $N_{\rm H}$ alone. Consequently, we imposed the temperature of the NS surface, the power-law slope $\Gamma$ and its normalization to be the same between different spectra, but free to vary. We get $\chi^2_\nu = 2.1$ for 193 d.o.f. We conclude that a change in $N_{\rm H}$ alone cannot account for the observed spectral change. Then, we verified that the spectral changes cannot be due to the variation of only one component plus the $N_{\rm H}$. By leaving both parameters of the power law free to vary between the different spectra, imposing the NS temperature to be the same, we get $\chi^2_\nu = 1.25$ (191 d.o.f.), while by leaving free the NS atmosphere temperature, imposing the power law (both parameters) to be the same, we get $\chi^2_\nu = 1.52$ (193 d.o.f.). Then, we left the power law (both $\Gamma$ and the normalization) and the NS atmosphere temperature free to vary, together with the $N_{\rm H}$, and we get a better fit, $\chi^2_\nu = 1.00$ for 189 d.o.f. The latter model is statistically significant at $5.4\sigma$ confidence level compared to when the power law alone is free to vary (*F*-test). We conclude that both spectral components must change, matching the conclusions of Cackett et al. (2010a).

By leaving both components free to vary, we measure $N_{\rm H} = 8.0 \pm 0.8 \times 10^{20}\,\mathrm{cm^{-2}}$, which is slightly lower than the total Galactic column density in the source direction (Dickey & Lockman 1990; Kalberla et al. 2005, $8.4 - 9.2 \times 10^{20}\,\mathrm{cm^{-2}}$), and slightly higher than that found by Cackett et al. (2010a), however, consistent within cross-calibration uncertainty between different satellites (e.g. Tsujimoto et al. 2011). The effective NS atmosphere temperature measured at infinity was found to decrease with the flux: $kT_{\rm h} = 80 \pm 2$ eV, $kT_{\rm m} = 73.4 \pm 0.9$ eV and $kT_{\rm l} = 59 \pm 1.5$ eV. We found a slightly higher value for the power-law spectral index in the case of the low count spectrum, where $\Gamma_{\rm l} = 2.0 \pm 0.2$. However, within the $3\sigma$ of the statistical uncertainty it is consistent to be constant, since $\Gamma_{\rm m} = 1.4 \pm 0.2$ and $\Gamma_{\rm h} = 1.4 \pm 0.5$. Only the temperature of the thermal component and the power-law normalization are clearly changing (see Table 4). Since we are mapping here the Wein tail of the thermal component (that peaks at ∼0.18 keV), this is equivalent with saying that, within statistical uncertainty, the overall spectral shape is constant and only the flux is changing, meaning that the *nsatmos* model is moving only up and down in the plot (see Fig. 5). Indeed, by imposing that $\Gamma$ is constant between the three spectra, but free to vary, we get a statistically acceptable fit ($\chi^2_\nu = 1.03$, 191 d.o.f.), with $\Gamma = 1.7 \pm 0.15$, and all other model components consistent with the previous fit within statistical uncertainty.

**Table 4.** Main spectral results as a function of the count rate: low $<0.07\,\mathrm{c\,s^{-1}}$, medium 0.07–0.11 $\mathrm{c\,s^{-1}}$ and high $>0.11\,\mathrm{c\,s^{-1}}$. The three spectra are fitted together, with a total $\chi^2_\nu$ for 100 d.o.f. The measured column density, imposed to be the same in the three spectra, is $8.0 \pm 0.8 \times 10^{20}\,\mathrm{cm^{-2}}$. We assumed an NS mass of 1.4 $\mathrm{M_\odot}$, a radius of 10 km and a distance of 1.2 kpc. The normalization of the power law is defined as photons $\mathrm{keV^{-1}\,cm^{-2}\,s^{-1}}$ at 1 keV. We also reported the thermal fraction, the 0.5–10 keV unabsorbed flux and the extrapolated 0.01–100 keV unabsorbed flux, and the derived 0.01–100 keV luminosity at 1.2 kpc, all for both components summed together, and the 0.01–100 keV unabsorbed (bolometric) flux for the thermal component only. Uncertainties are $1\sigma$ confidence level.

| Parameter | Unit | High | Medium | Low |
|---|---|---|---|---|
| $kT^\infty$ | eV | $80 \pm 2.0$ | $73.4 \pm 0.9$ | $59 \pm 1.5$ |
| $\Gamma$ | | $1.4 \pm 0.5$ | $1.4 \pm 0.2$ | $2.0 \pm 0.2$ |
| Norm. | $10^{-4}$ | $2^{+1.7}_{-1.0}$ | $1.5 \pm 0.4$ | $1.3 \pm 0.3$ |
| Thermal ratio | per cent | $62 \pm 6$ | $59 \pm 4$ | $51 \pm 5$ |
| $F^{\rm total}_{0.5-10\,\rm keV}$ | $10^{-12}$ erg s$^{-1}$ cm$^{-2}$ | $5.0 \pm 0.5$ | $3.5 \pm 0.2$ | $1.3 \pm 0.2$ |
| $F^{\rm total}_{0.01-100\,\rm keV}$ | $10^{-12}$ erg s$^{-1}$ cm$^{-2}$ | ∼14 | ∼11 | ∼3.5 |
| $F^{\rm thermal}_{0.01-100\,\rm keV}$ | $10^{-12}$ erg s$^{-1}$ cm$^{-2}$ | $5.2 \pm 0.4$ | $3.7 \pm 0.2$ | $1.5 \pm 0.1$ |
| $L^{\rm total,\,1.2\,kpc}_{0.01-100\,\rm keV}$ | $10^{33}$ erg s$^{-1}$ | ∼2.4 | ∼1.9 | ∼0.6 |
| $L^{\rm thermal,\,1.2\,kpc}_{0.01-100\,\rm keV}$ | $10^{32}$ erg s$^{-1}$ | $9.0 \pm 0.7$ | $6.4 \pm 0.7$ | $2.6 \pm 0.2$ |
| $\chi^2_\nu$ (d.o.f.) | 1.00 (100) | | | |

To further assess if the spectral shape is really constant as the flux varies, we compared, for each XRT observation, the 0.3–2 keV count rate with that in the 2–10 keV energy band, where the thermal and power-law components are, respectively, dominating the total flux. This has the advantage of allowing us to see changes between every daily observation rather than looking at just the three high, medium and low count spectra. We show this count rate–count rate diagram in Fig. 4, and it shows a tight linear relation. We found the best fit for the data to be a constant plus a linear function with a constant value of $-8 \pm 4 \times 10^{-4}$ and a slope of $0.123 \pm 0.007$ ($\chi^2_\nu = 1.14$ for 56 d.o.f.). Since a linear model perfectly fits the data this implies that the overall spectral shape remains constant as the flux changes, meaning that $kT$ is varying and the power-law normalization is changing as well and in such a way to compensate the temperature change of the thermal component.

We defined the thermal ratio as the fraction of the unabsorbed 0.5–10 keV thermal flux to the total unabsorbed 0.5–10 keV flux. From the fit with the power-law index free we get a thermal ratio of $62 \pm 6$, $59 \pm 4$ and $51 \pm 5$ per cent in the case of high, medium and low count rate, respectively. While, by imposing the power-law slope to be the same among different spectra the thermal ratio is more

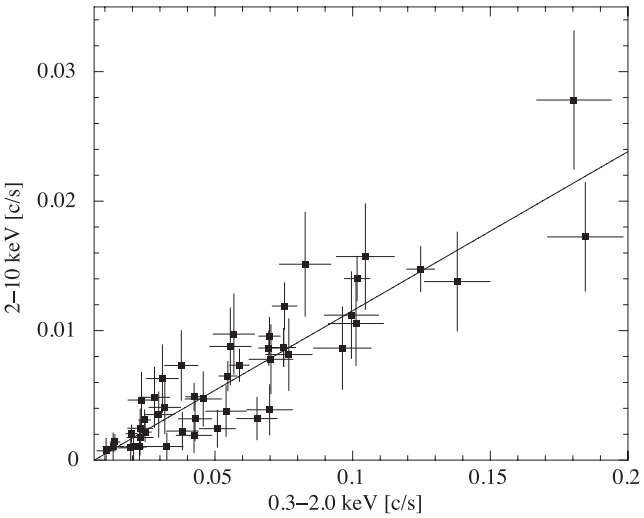


**Figure 4.** 0.3–2.0 keV count rate versus 2–10 keV count rate. The solid line represents the best straight-line fit.

constant and it is 59 ± 5, 55 ± 5 and 54 ± 4 per cent, respectively. We conclude that both components are always responsible for about the same fraction (∼50 per cent) of the total unabsorbed 0.5–10 keV flux, and they are changing in tandem. In order to get an estimate of the mass accretion rate, we also extrapolated the spectral model in the 0.01–100 keV energy range, and reported the estimated total flux and luminosity together with that of the thermal component only in Table 4.

We note the presence of a feature at about ∼0.7 keV in the residual of the low count rate spectrum (see Fig. 5). If it is modelled with an absorption Gaussian (*gabs*) we get an energy of 0.68 ± 0.01 keV, a line width ($\sigma$) of 40 ± 20 eV and an optical depth ($\tau$) at line centre of 0.08 ± 0.02. The value of $N_{\rm H}$ is slightly lower than in the case of the fit without the absorption Gaussian and it is $6.3 \pm 0.8 \times 10^{20}$ cm$^{-2}$, while all other model parameters are consistent within $1\sigma$ of the statistical uncertainty. The fit has a $\chi^2_\nu = 0.87$ with 186 d.o.f. The inclusion of the Gaussian has a single-trial significance of $4.8\sigma$, however, including the number of spectra and spectral bins searched to find this feature reduces the significance greatly. This is the first time that this kind of feature is observed in the spectrum of Cen X-4. There are several possible lines close to an energy of 0.68 keV (see e.g. Verner et al. 1996). In the case that the gas around the NS is in an ADIOS state, an outgoing wind can form driving away matter from the compact object. This is an alternative scenario to the ADAF solution which always involve a radiatively inefficient accretion flow. If such a wind is present, O VIII might be the strongest line detected in the spectrum. From the optical depth of the line we estimated the equivalent hydrogen column density due to a possible outgoing wind. Since $\tau = N\sigma_{\rm c}$, where $N$ is the column density and $\sigma_{\rm c}$ is the Thompson cross-section ($6.65 \times 10^{-25}$), we get $N_{\rm H} = 1.20 \times 10^{23}$ cm$^{-2}$. This is a very large value, a factor of about 150–200 above the photoelectric absorption due to the interstellar medium. Such a dense wind would likely have other observable absorption lines that we do not see, though detailed photoionization modelling would be needed to test this. Given the high density and the lack of this feature in any previous observations of Cen X-4, it is likely not a real detection.

Finally, as a further check of the goodness of the choice of the *nsatmos* model (see also Rutledge et al. 1999 for a justification of using NS atmosphere models rather than a simple blackbody, BB), we verified that the radius $R$, always assumes meaningful values, meaning that it is always consistent with the emission from the NS surface (e.g. is not greatly above 15 km). Consequently, we left $R$ as a free parameter and we estimate its uncertainty at $3\sigma$. We imposed that the atmosphere temperature is the same between different spectra, but left $R$ free to vary and we also imposed $N_{\rm H} = 8.0 \times 10^{20}$ cm$^{-2}$. We obtained an average effective temperature of 66 ± 4 eV and $R_{\rm h} = 13 \pm 4$ km, $R_{\rm m} = 12 \pm 4$ km and $R_{\rm l} = 8 \pm 2$ km ($\chi^2_\nu$ 0.96 for 189 d.o.f.). We conclude that $R$ is always consistent with the emission from the surface of an NS (∼9−15 km). If instead we fix $R$ = 10 km and leave the *nsatmos* normalization free (this

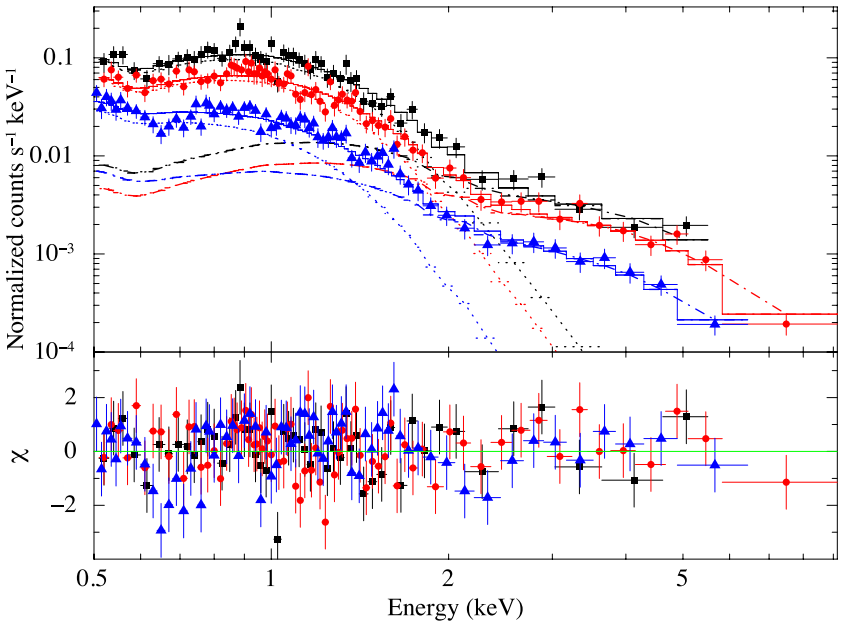


**Figure 5.** Summed spectra of Cen X-4 for three count rate ranges: low <0.07 c s$^{-1}$ (blue triangles), medium 0.07–0.11 c s$^{-1}$ (red circles) and high >0.11 c s$^{-1}$ (black squares). The solid line represents the total model, while the dotted line represents the *nsatmos* component and the dash-dotted line the power-law component. Model residuals are showed in the lower panel.

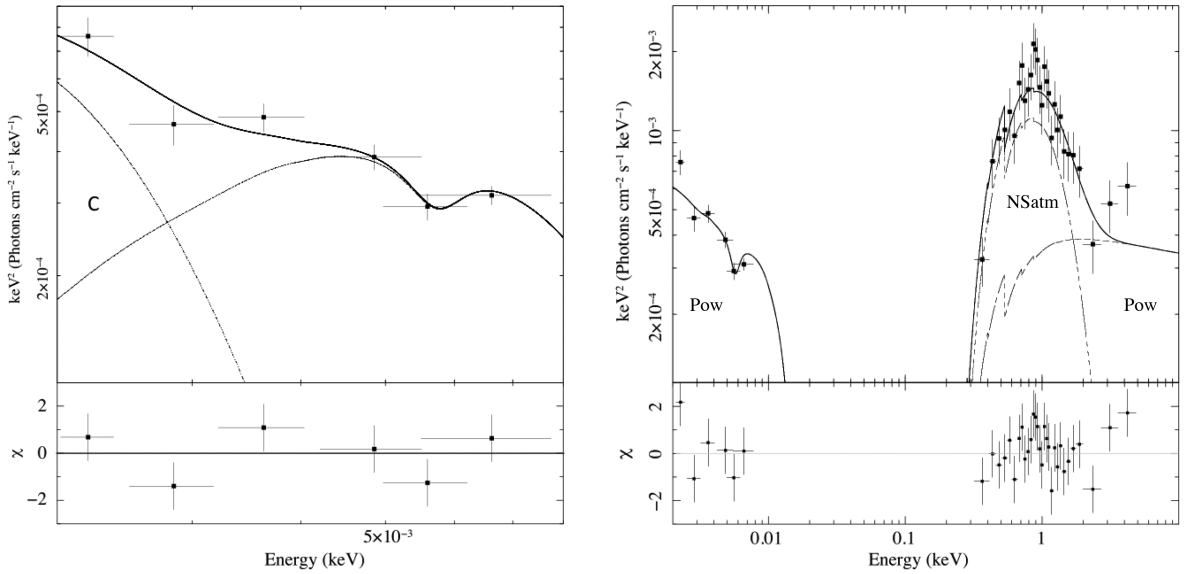


**Figure 6.** Left-hand panels: two BB spectral fit in the optical and UV energy range. The dotted lines represent the two BB components (that of the companion star, on the left of the plot, is marked with a C), while the continuum line represents the total model. In the lower panel model residuals are shown. Right-hand panels: SED fit from optical up to the X-ray band. A fit with a model comprised of an NS atmosphere (*nsatm*), accounting for the soft X-ray photons ($E < 2$ keV), plus a power law (Pow), extending from the optical up to the hard X-ray band and dominating in the optical and *UV* bands and in the hard X-ray band ($E > 2$ keV), is shown. In the case of an ADAF model, the synchrotron emission dominates up to 0.01 keV (substituting the low energy tail of the power law) while the bremsstrahlung dominates above 2 keV (substituting the hard energy tail of the power law).

parameter defines the fraction of the NS surface which is emitting) its value is always consistent with one, within statistical uncertainty.

### 4.6 Spectral energy distribution and energetics

We studied the SED from the optical to the X-ray band. We have 10 pointings in which *Swift* was observing in all the UVOT band, so we selected the X-ray brightest (obsid 00035324019, $0.137\,\mathrm{c\,s^{-1}}$) of these 10 pointings in order to get the best S/N possible (we cross-checked the results with that of another bright pointing among these 10, obsid 00035324050, $0.080\,\mathrm{c\,s^{-1}}$). We fixed the reddening at $E(B-V) = 0.1$ (Chevalier et al. 1989) using the *redden* model in XSPEC. We downloaded the correct response matrix file for each filter from the *Swift* web page.[3] We first fitted the UVOT data alone testing the scenario of a companion star (optical) plus an accretion disc (UV). We used a model comprised of two BB, one accounting for the companion star, *c*, at the fixed temperature of $3.88 \times 10^{-4}$ keV (González Hernández et al. 2005, 4500 K), and another one accounting for the disc, *d*, with both its parameters free. Then, we tested a model made by the sum of a BB (accounting for the companion star) with the temperature fixed plus a disc BB with all component free. For the two BB model we get: $R_\mathrm{c} = 0.50 \pm 0.05\,\mathrm{R}_\odot$, $kT_\mathrm{d} = 0.0014 \pm 0.0001$ keV ($16\,000 \pm 1400$ K) and $R_\mathrm{d} = 24200 \pm 200$ km, assuming a distance of 1.2 kpc, with a $\chi^2_\nu = 1.87$ for 3 d.o.f. (see Fig. 6). For the BB plus disc BB model we get $R_\mathrm{c} = 0.43 \pm 0.06\,\mathrm{R}_\odot$, $kT^\mathrm{inn}_\mathrm{disc} = 0.0024 \pm 0.0004$ keV ($28000 \pm 4500$ K) and $R^\mathrm{inn}_\mathrm{disc} = 8000 \pm 3000$ km (assuming a disc inclination of 30°), where $kT^\mathrm{inn}$ is the temperature of the inner disc and $\mathrm{R}^\mathrm{inn}$ is its realistic radius (see Kubota et al. 1998, for the correction factor between the apparent inner disc radius and the realistic radius), with a $\chi^2_\nu = 1.75$ for 3 d.o.f. We note that for both models, the fit is insensitive to $kT_\mathrm{c}$ if it is left free to vary, moreover, the $\chi^2_\nu$ is not satisfactory. However, the majority of the residual contribution is arising from the two optical points, where the companion star is dominant. This is not surprising since, here, we are modelling the K3–7 V star with an extremely simplified model, consisting of a pure BB emission. We note that a companion star with a radius of $1.2\,\mathrm{R}_\odot$ is inconsistent with our results, which would instead favour a value of $0.5\,\mathrm{R}_\odot$, fully compatible with the lower estimate of González Hernández et al. (2005).

We also fitted the whole SED, from the *O* to the X-ray band. In order to first test the scenario proposed by Campana & Stella (2000) of a quenched radio pulsar emission, which would result in a single power law extending from the optical up to the X-ray band, we started fitting the SED using a single power law plus an NS atmosphere (*nsatmos*) model (to account for the NS surface thermal emission), all multiplied by the reddening (*redden*) and the interstellar absorption (*phabs*). We fixed the value of following parameters: $N_\mathrm{H} = 8 \times 10^{20}\,\mathrm{cm^{-2}}$ (average X-ray spectral value), $E(B-V) = 0.1$ (known reddening), $R_\mathrm{NS} = 10$ km, $M_\mathrm{NS} = 1.4\,\mathrm{M}_\odot$ and $d = 1.2$ kpc (see Section 4.5). The power law (left free to vary) has a photon index $\Gamma = 2.10 \pm 0.03$, and intercepts the optical, UV and hard X-ray points (see Fig. 6). We note that the inclusion of a BB component to account for the companion star is not statistically required, because the power law dominates in the optical band. This is due to the fact that we have only two spectral points in this band. However, a $3\sigma$ upper limit to the radius of the companion star is $0.4\,\mathrm{R}_\odot$ (close to the lower estimate of $0.5\,\mathrm{R}_\odot$ reported by D'Avanzo et al. 2005). The model provides a statistically acceptable fit, $\chi^2_\nu = 0.95$ (33 d.o.f.).

Secondly, conscious of the limited number of data points in the *UV* band, we only tried to put some constrain on the ADAF scenario using a model made by the sum of a Comptonized BB emission (*compbb*), plus synchrotron emission (*srcut*), plus a bremsstrahlung (*bremss*), plus an NS atmosphere (*nsatmos*), all multiplied by the reddening (*redden*) and the interstellar absorption (*phabs*). Comptonization, synchrotron and bremsstrahlung are the three most efficient cooling mechanisms expected in an ADAF for an NS LMXB.

[3] swift.gsfc.nasa.gov

**Table 5.** Estimated flux in the *O–UV* filter bandpass for obsid 00035324019. The corresponding $\nu F_\nu$ value is also reported. Uncertainties are $1\sigma$ confidence level.

| Filter | $\nu$ $10^{14}$ (Hz) | Flux $10^{-13}$ (erg cm$^{-2}$ s$^{-1}$) | $\nu F_\nu$ $10^{-13}$ (erg cm$^{-2}$ s$^{-1}$) |
|---|---|---|---|
| *UVW*2 | 15.5 | $4.4 \pm 0.2$ | $5.3 \pm 0.2$ |
| *UVM*2 | 13.3 | $2.9 \pm 0.2$ | $4.9 \pm 0.3$ |
| *UVW*1 | 11.5 | $3.2 \pm 0.3$ | $6.0 \pm 0.4$ |
| *U* | 8.7 | $3.0 \pm 0.2$ | $7.9 \pm 0.7$ |
| *B* | 6.8 | $2.6 \pm 0.3$ | $7.6 \pm 0.7$ |
| *V* | 5.5 | $2.4 \pm 0.2$ | $12 \pm 1$ |

The Comptonization is expected to dominate close to the NS while the bremsstrahlung is dominating further out, both mechanisms produce X-ray photons. The contribution of the synchrotron is relevant close to the NS and is emitting in the UV (Narayan & Yi 1995b). We fixed the value of the following parameters: $N_{\rm H} = 0.08 \times 10^{20}$ cm$^{-2}$ (average X-ray spectral value); $E(B-V) = 0.1$ (known reddening); $kT_{\rm seed} = 0.08$ keV (NS surface temperature from spectral fit) and $kT_{\rm e} = 86$ keV, norm $= 1 \times 10^{10}$ (as expected for a hot electron Comptonizing medium close to the NS surface emitting at $L = 2.4 \times 10^{33}$ erg s$^{-1}$, for a distance of 1.2 kpc, see Narayan & Yi 1995b), where $kT_{\rm seed}$ is the temperature of the seed photons, $kT_{\rm e}$ is the temperature of the hot electrons and norm $= (L_{39}/D_{10})^{1/2}$ is the normalization;[4] $kT_{\rm bremms} = 8.6$ keV (as expected for cooler electrons far from the NS at a distance of $\sim$6200 Schwarzschild radii; Narayan & Yi 1995b, and see also Section 5.4.3 for a discussion of this number). We found the fit to be insensitive to $\alpha$, which is the spectral index of the synchrotron emission, that consequently we fixed to 1. We also found the break frequency of the synchrotron to be largely uncertain, a lower limit on it being $1.5 \times 10^{15}$ Hz. This is not surprising since the shape of the observed SED does not show any break in the observed bands, and the flux slowly decreases with the frequency. Consequently, we arbitrarily fixed the break frequency at $2 \times 10^{15}$ Hz, just above the limit of the explored frequency (see Table 5). Moreover, the optical depth ($\tau$) of the Comptonizing plasma is also unconstrained. This is because the contribution of this component is minimal both in the optical and UV, where the synchrotron is dominating, than in the hard X-ray ($E > 2$ keV), where the bremsstrahlung is dominating (see Fig. 6). Consequently, we removed this component from the total model. The resulting model (NS atmosphere+synchrotron+bremsstrahlung) provides a good fit with $\chi^2_\nu = 0.97$ with 33 d.o.f. We note that, also in this case, the presence of a BB to account for the companion star is not statistically required, indeed the synchrotron emission dominates at optical wavelength. The $3\sigma$ upper limit to the radius of the companion star is $0.3\,{\rm R}_\odot$.

In order to estimate the total flux in the *O* and *UV* bands, we convert the flux densities (erg s$^{-1}$ cm$^{-2}$ Å$^{-1}$), that are the output of *uvotsource*, to fluxes by multiplying by the full width at half-maximum of the filter bandpass. We use 769 Å (*V*), 975 Å (*B*), 785 Å (*U*), 693 Å (*UVW*1), 498 Å (*UVM*2) and 657 Å (*UVW*2; Poole et al. 2008). Single flux estimates are reported in Table 5. We deredden the optical and UV fluxes using the gas-to-dust ratio, $N_{\rm H}({\rm cm}^{-2}) = 6.86 \times 10^{21}\,E(B-V)$, from Güver & Özel (2009) in order to convert the equivalent hydrogen column to $E(B-V)$. Then we use the interstellar extinction curve of Cardelli, Clayton & Mathis (1989) to estimate the extinction correction at the wavelengths of each filter. Consequently, we get the following conversion factors for each filter: 1.396 (*V*), 1.552 (*B*), 1.702 (*U*), 2.054 (*UVW*1), 2.677 (*UVM*2) and 2.432 (*UVW*2).

We obtain a UV (except *UVM*2) flux of $1.06 \pm 0.04 \times 10^{-12}$ erg cm$^{-2}$ s$^{-1}$, an optical ($B+V$) flux of $0.50 \pm 0.04 \times 10^{-12}$ erg cm$^{-2}$ s$^{-1}$, and, consequently, a total UV plus optical flux of $1.56 \pm 0.06 \times 10^{-12}$ erg cm$^{-2}$ s$^{-1}$. We did not include the *UVM*2 filter contribution, since it completely overlaps with the *UVW*2 and *UVW*1 bands. In order to compare simultaneous O, UV and X-ray flux measure, we also estimated the total unabsorbed X-ray flux. Since the hot NS surface is expected to emit below 0.5 keV, while the power law is likely extending above 10 keV, we extrapolated our model to a wider energy range corresponding to 0.01–100 keV. Since most part of the 10–100 keV flux is due to the power-law component, a small change in its slope can consistently affect the estimated flux. Consequently, we fixed $\Gamma = 1.4$, that is the value obtained on the average high count rate spectrum (and this observation is part of it). If we consider the uncertainty on the measure of the power-law slope, $\Delta\Gamma = 0.5$, we get an X-ray flux ranging from $\sim 4.6 \times 10^{-12}$ up to $\sim 5.1 \times 10^{-11}$ erg cm$^{-2}$ s$^{-1}$. Taking into account the uncertainty on the X-ray flux estimate we get that the ratio between UV and X-ray flux has to be $2.1 < F_{\rm UV}/F_{\rm X} < 23$ per cent.

## 5 DISCUSSION

### 5.1 Evidence for accretion

We showed that the X-ray and UV light curves of Cen X-4 during quiescence are both highly variable, with the fractional root-mean-square variability $F_{\rm var} = 73.0 \pm 1.5$ and $50.0 \pm 1.4$ per cent, respectively, while the optical light curve is changing less ($F_{\rm var} = 10.0 \pm 1.6$ per cent). The first-order X-ray and *UVW*1 structure function ($V_\tau$) shows the shape expected for a power spectrum with index $-2$ (red noise), as is typically seen in accreting systems (two plateau connected by a power law). The time-scale of the variability underlying the structure function goes from few days ($\sim$5) up to months. The excess in the structure function at about 5 d is likely connected to the peaks which are present in the X-ray and *UVW*1 light curves at about 40, 50, 70, 90 and 110 d, whose average rise and decay time is indeed about 5 d. In the time between different peaks the count rate seems to always reach a minimum (ground) level extremely close to the detection limit for both the X-ray and the *UVW*1 band. We observed the strongest X-ray variability on short time-scale ever detected for Cen X-4 during quiescence[5] a factor of 22 and a factor of 13 in only 4 d (between 97.2 and 101.5 d and between 39.5 and 43.3 d, respectively). This is much higher than previously reported by Campana et al. (1997), who found a factor of $\sim$3 on a time-scale of 4 d and Cackett et al. (2013a) who found a factor of $\sim$3 change in 7 d.

Moreover, we showed that both the spectral components, the NS atmosphere and the power law, must change with the flux. We also showed that they are changing in tandem, implying that they are

[4] $L_{39}$ is the luminosity in unit of $10^{39}$ erg s$^{-1}$ and $D_{10}$ is the distance in unit of 10 kpc.

[5] We are not considering here X-ray bursts detected from Cen X-4 immediately before outbursts began or the X-ray flare in 1971 detected by Apollo 15 that could have been an X-ray burst from Cen X-4 (Kuulkers et al. 2009). The association with Cen X-4 is not certain and is impossible to establish if the source was truly in quiescence at that time.

closely linked. While this has previously been shown for time-scales of months to years (Cackett et al. 2010a), this is the first demonstration on time-scales of days. A change in the thermal component that we detected as a surface temperature change strongly suggests that the accreting matter must reach the surface of the NS, overtaking the centrifugal barrier of the rotating magnetosphere. Since the two spectral components are so closely linked, accretion must be, very likely, also responsible for the change in the power law. A very low level of accretion seems to occur quite continuously, generating random episodes of high count rates and consequently modifying the temperature of the surface, which is hotter when the count rate is higher. We emphasize that, assuming the NS atmosphere model to be the correct model to fit the data, we obtain a radius which is less than 15 km. This is encouraging in considering the X-ray emission as arising from the NS itself. The scenario proposed by e.g. Campana & Stella (2000), where the X-rays are produced at the shock point between a radio pulsar wind and the inflowing matter from the donor star, is for Cen X-4 likely disfavoured. While this scenario can account for the single power law extending from the *O–UV* up to the X-ray band, according to its prediction only the power-law component should change, which is not the case. We note that it is extremely difficult to account for such intense, non-monotonic, multiflare-like variability, with a clear correlation between the thermal and power-law spectral component, without invoking accretion that is somehow occurring at very low Eddington luminosity rates in Cen X-4. However, we emphasize that for other quiescent sources, where e.g. the thermal and power-law emission are not so closely correlated, accretion may not be the right scenario.

When matter is accreted on to the NS surface it can emit a thermal-like spectrum (Zampieri et al. 1995), that is harder than a BB emission at the NS effective temperature, moreover, it also emits a consistent excess in the Wien tail region. At the level of S/N of our data, this perfectly matches the characteristics of an NS atmosphere model (see Soria et al. 2011 for more details about the comparison between different thermal models). Cen X-4 is not the only NS LMXB showing quiescent variability, other examples are Aql X-1 and EXO 1745−248 (see e.g. Cackett et al. 2011; Degenaar & Wijnands 2012, and references therein), but at present it is the source showing the most intense variation on short time-scales (4 d). More recently, SAX J1750.8−2900 showed evidence of a small flare, with flux increase of a factor of 10 above the quiescent level (Wijnands & Degenaar 2013), lasting less than 16 d, suggesting that also in this case low level of accretion can occur in quiescence at least during these flare episodes (see also Fridriksson et al. 2011 for a similar flare from the transient NS XTE J1701−462). This kind of flare is reminiscent of the peaks in the count rate we are observing from Cen X-4. They both last several days, however, Cen X-4 has a less intense emission, $L = 10^{32-33}$ erg s$^{-1}$ (compared to $10^{34}$−$4 \times 10^{34}$ erg s$^{-1}$). We can detect and explore this kind of variability, occurring at low X-ray luminosity, only for Cen X-4, because it is relatively close to us.

### 5.2 Remarks about past and future quiescent studies

We emphasize that, because of the strong intensity change in the UV and X-ray count rate we observed here, any kind of study of the quiescent emission of Cen X-4, and of LMXB in general, must be based on simultaneous multiwavelength (e.g. O, UV and X-ray) data only. Recently, Hynes & Robinson (2012) pointed out that a promising method to discriminate between BH and NS LMXB is to compare their X-ray versus UV luminosity ratio, with the NS exhibiting $L_{\rm X}/L_{\rm UV}$ a factor of 10 times higher. However, only two sources in this study had simultaneous X-ray and UV observations (note that Hynes & Robinson 2012, do caution about the use of non-simultaneous data). We showed that using non-simultaneous data can easily introduce an error of at least a factor of ∼22 in the estimate of the ratio. The same kind of consideration and caution also applies to any other multiwavelength quiescent study where non-simultaneous data are used.

If accretion is still occurring also at low Eddington luminosity rates for Cen X-4, this would imply that any intrinsic cooling emission from the NS should be equal to or less than the observed $kT$ in the lowest count rate spectrum, 59.0 ± 1.5 eV. In cooling NS studies, the quiescent bolometric thermal luminosity (e.g. 0.01–100 keV), that for Cen X-4 we measured to be $\leq 2.6 \times 10^{32}$ erg s$^{-1}$, can be compared with the estimated time-averaged mass transfer rate to find the most likely cooling scenarios among the several that are currently available (see e.g. Heinke et al. 2009; Wijnands, Degenaar & Page 2013, and references therein). The literature value of the surface temperature of Cen X-4 used for these kind of studies, $kT = 0.76$ (Heinke et al. 2007), is higher than that we measure here for the low count rate spectrum, consequently also the inferred luminosity is higher $4.8 \times 10^{32}$ erg s$^{-1}$. Moreover, we also note that the time-averaged mass transfer rate is derived under the condition that the time-averaged mass accretion rate over the last 10 yr is reflecting the time-averaged mass transfer rate. However, we have shown that the emission from Cen X-4 in quiescence is highly variable, with count rate variation of at least a factor of 22 in only a few days. Summarizing, we emphasize that to perform an accurate study of the cooling mechanism of Cen X-4 a temperature ≤59 eV, and an 0.01–100 keV bolometric thermal luminosity $\leq 2.6 \times 10^{32}$ erg s$^{-1}$, should be considered.

### 5.3 Magnetospheric accretion without a strong propeller?

Models of accretion flows around quiescent NSs like Cen X-4 typically assume that the source is in a 'strong propeller' regime (Illarionov & Sunyaev 1975), in which the rapidly spinning magnetosphere of the star creates a large centrifugal barrier that drives an outflow and inhibits accretion on to the star. The persistent X-ray emission and rapid variability seen in Cen X-4 and other sources challenge this assumption.

Furthermore, Asai et al. (1998) and Menou et al. (1999b) have suggested that a powerful propeller effect is necessary to make an ADAF model compatible with observations of quiescent NSs. This is because ADAFs radiate very inefficiently but accrete at a relatively high rate even in quiescence ($\sim 10^{-2}$−$10^{-3}\dot{M}_{\rm Edd}$). The ADAF picture should apply to both quiescent NSs and BHs, except that NSs will have a much higher radiative efficiency than BHs, since all the matter advected through the flow will end up on the surface of the star. To reconcile this fact with the low quiescent luminosities of NSs like Cen X-4 ($\sim 10^{-5} L_{\rm Edd}$), Menou et al. (1999b) have suggested that the vast majority (up to ≃99.9 per cent) of the accretion flow around the star is expelled through the propeller effect.

However, Cen X-4 likely has a low magnetic field, indicating that a strong propeller is unlikely to be operating at the accretion rates implied by the ADAF scenario. In order for matter to be expelled in a propeller, the 'magnetospheric radius' (where the magnetic field is strong enough to truncate the disc) must significantly exceed the corotation radius ($r_{\rm c} \equiv (GM_*/\Omega_*^2)^{1/3}$, where $M_*$ is the mass of the star and $\Omega_*$ its spin frequency), the radius at which the Keplerian rotation in the disc equals the spin of the star (Spruit & Taam 1993). Here, we assume (favourably for a propeller to form) that Cen X-4 has a spin period of ∼2.5 ms and the magnetic field is of the order

of $10^9$G (still small enough to be overwhelmed by $\dot{M}_{\rm Edd}$ so that pulsations are not seen in outburst; in reality fields $\sim 10^7$–$10^8$ G are more likely). If $\dot{M} \simeq 10^{-2}\dot{M}_{\rm Edd}$ through the flow as it approaches the star (with 0.1 per cent of that eventually accreting on to the star), the accretion flow will be truncated around

$$r_{\rm m} = 6.3 R_* \frac{\xi}{0.52}\left(\frac{B}{10^9{\rm G}}\right)^{4/7}\left(\frac{0.01}{\dot{M}_{\rm Edd}}\right)^{-2/7}\left(\frac{M_*}{1.4\,{\rm M}_\odot}\right)^{-1/7}. \quad (2)$$

In this equation (taken from Ghosh & Lamb 1979), $R_*$ is the NS radius, $B$ is the surface magnetic field and $\xi$ is a factor of order unit to account for uncertainties in the interaction between the flow and stellar magnetic field. Therefore, even under favourable circumstances, $r_{\rm m} \sim 2r_{\rm c}$, which is unlikely to produce such a strong propeller as needed in this picture. Recent simulations of the propeller regime find $\dot{M}_{\rm acc}/\dot{M}_{\rm ej} \sim 0.04$ (the ratio of accreted to ejected material) for a considerably stronger propeller ($r_{\rm m} \sim 5r_{\rm c}$; Lii et al. 2013). Moreover, the ratio between accreted and ejected matter (and how it scales with $r_{\rm m}/r_{\rm c}$) is extremely uncertain, making it essentially impossible to predict the mean accretion rate through the flow from the amount that ends up on the star.

The extremely low accretion/ejection ratio required by the propeller ADAF model also presents a challenge for mass-loss from the donor star. We estimated that over the last 40 yr Cen X-4 accreted $\sim(4-7) \times 10^{24}$ g during its two outbursts and $\sim 10^{25}$ g during quiescence (assuming $\dot{M}_{\rm acc}/\dot{M}_{\rm ej} \sim 10^{-3}$, i.e. the outflow rate is 1000 times larger than the observed accretion rate). This implies a mass transfer rate of $2 \times 10^{16}$ g s$^{-1}$. Without an outflow, the transfer rate is (3–6) $\times 10^{15}$ g s$^{-1}$. Models for mass transfer through Roche lobe overflow suggest transfer rates of at most (2–7) $\times 10^{15}$ g s$^{-1}$ (Menou et al. 1999b; although they note enhanced accretion from magnetic braking is possible).

An alternative scenario ('dead disc') to the strong propeller was recently presented in D'Angelo & Spruit (2010, 2012). Following from an earlier suggestion of Spruit & Taam (1993), they note that for $r_{\rm m} < 1.3r_{\rm c}$ (which could likely be the case of Cen X-4) the interaction with the magnetic field will not be enough to unbind the disc into an outflow, so that material at $r_{\rm m}$ will instead remain bound, adding the angular momentum it acquired to the accretion flow. More significantly, in this scenario the inner edge of the accretion flow remains always very close to $r_{\rm c}$, and thus allows accretion on to the star, even at very low accretion rates. Meaning that the magnetosphere holds back material in the flow, but some small amount accretes on to the star. This may naturally explain the low-level quiescent emission seen in Cen X-4, which could then be a reflection of $\dot{M} \simeq 10^{-5}$–$10^{-6}\dot{M}_{\rm Edd}$ in the inner regions of the flow. This can happen in principle both for an ADAF and for a thin disc scenario, however, a note of caution: the solutions of D'Angelo & Spruit (2010) were formally calculated assuming a thin accretion disc, and may be significantly altered for an ADAF-type solution.

In order for the scenario outlined by Menou et al. (1999a) to still be viable, the vast majority (99.9 per cent) of the mass in an ADAF must be expelled before it reaches the magnetosphere of the NS. This must then apply equally to ADAFs around NSs and BHs, and support models (see e.g. Blandford & Begelman 1999, about the ADIOS model) in which most matter in a radiatively inefficient flow is expelled before it accretes on to the central object by an intense outgoing wind intrinsic to the accretion flow itself.

### 5.4 Origin of the UV emission

In quiescent LMXBs the donor stars are considered intrinsically too cool to have any significant UV emission (e.g. Hynes & Robinson 2012). The UV, then, could probe the emission from a particular region of the accretion flow. However, the exact location of origin of the UV emission in the accretion flow is still unclear and it is consequently debated. The UV emission could arise due to: (I) the thermal emission from the gas stream impact point, (II) the thermal emission from a standard, optically thick and geometrically thin accretion disc truncated far from the compact object, (III) the emission from an ADAF, or alternatively the UV emission could be due to (IV) X-ray irradiation of, and reprocessing (perhaps in the inner accretion disc or on the surface of the companion star). We will explore in detail the different scenarios in the following section.

#### *5.4.1 Thermal emission from the gas stream impact point*

Our analysis clearly showed that the UV and the X-ray emissions are strongly correlated. Signs of a correlation were first noticed by Cackett et al. (2013a). However, thanks to our long-term multiwavelength monitoring campaign, we had the chance to deeply explore the nature of this correlation. We find that X-ray and UV emissions are correlated on long time-scale, $t \leq 5$ ks (corresponding to an XRT pointing), on short time-scale, $t \leq 2$ ks (corresponding to an UVOT snapshot), and also on very short time-scale down to $t \leq 110$ s (corresponding to the shortest UVOT snapshots). Furthermore, we have been able to unveil for the first time the real shape of this correlation. Whenever enough data points are available so that the high X-ray count rate ($\gtrsim 0.17$ c s$^{-1}$) is covered, the shape of the correlation is a power law with spectral index 0.2–0.6. Moreover, also the optical $V$ band and X-ray emission are correlated, both on long and on short time-scales. The presence of a correlation, especially that at very short time-scales (110 s) clearly rules out the thermal emission from the stream impact point as source of the UV photons. Indeed, if we assume that the UV light is tracing the matter in the disc, UV variations would refer to instability propagation throughout the disc. However, the time-scale to traverse the whole disc from the stream impact point (where the matter lost by the companion star impact on the outer accretion disc) to the inner edge is significantly longer than the correlation time-scale, being of the order of several weeks (Frank et al. 2002). Such a long time-scale cannot explain any of the correlations we are observing here. These results are in contrast with what reported by McClintock & Remillard (2000) and Menou & McClintock (2001), who found the gas stream impact point as the most likely source of the UV emission for Cen X-4. However, they only suggested that the UV emission could be powered, in terms of total luminosity, by the estimated mass transferred by the companion star to the outer edge of the accretion disc. Nevertheless, they could not explore the consequences of variability, crucial to test this scenario, due to the lack of data at that time. In summary, the fact that the X-ray and UV emissions are correlated unambiguously rules out the stream impact point as source of the UV photons.

#### *5.4.2 Thermal emission from a truncated standard accretion disc*

No sign of the presence of an accretion disc has been seen in the X-ray spectrum of Cen X-4 during quiescence, or in LMXBs in general – the thermal component in quiescent NSs is always consistent with the NS itself, while quiescent BH just show power-law spectra. This suggests that, at very low mass accretion rate, the disc is likely not extending down to the NS surface, as occurs during outburst (where the disc is clearly emitting in the X-ray), but is likely truncated further out. Theoretical model gives support to the truncated disc scenario, suggesting that it is extremely easy for the matter in the inner part of the accretion disc, if the mass accretion

rate is very low (e.g. under a critical value that for NS is $\dot{M}_{\rm cr}/\dot{M}_{\rm Edd} \sim 10^{-2}$–$10^{-3}$), to evaporate and enter in a optically thin and radiatively inefficient spherical accretion flow state surrounding the compact object (Narayan & Yi 1995a,b; Narayan et al. 1998; Blandford & Begelman 1999). Moreover, the DIM model (Cannizzo 1993; Lasota 2001) requires the disc to be truncated during quiescence in order to explain transients. Based on the correlation results only, we now want to demonstrate that mass accretion rate fluctuations, propagating inwards from any point of a standard thin disc (e.g. Shakura & Sunyaev 1973), cannot be the reason for the X-ray variability observed here.

In the standard disc solution, the radial velocity of the matter in the disc is of the order of $0.3\,{\rm km\,s^{-1}}$ (Frank et al. 2002), and the measured time-scale of the correlation is $t \leq 110\,{\rm s}$. Consequently, if the observed correlation is generated by matter propagating in a standard disc, finally accreting on the NS surface, this matter must propagate from a maximum distance of about 33 km from the NS centre. However, this would imply that the disc is extending down to the NS surface which is not observed (the X-ray thermal emission is consistent with the emission from the NS surface only). Moreover, if we impose that the viscous time-scale, which is the time-scale on which matter moves through the disc under the influence of the viscous torque, is equal to the correlation time-scale, we could get an estimate of the size of the disc in an extremely peculiar scenario, where the dynamics in the disc would be fast enough to justify the observed correlation. The radius of the accretion disc as a function of the viscosity time-scale is given by (Frank et al. 2002)

$$R_{10} = \left(\frac{t_{\rm vis}}{3\times10^5}\right)^{4/5} \alpha^{16/25} m_1^{-1/5} (\dot{M}_{16})^{6/25}, \quad (3)$$

where $R_{10} = R/(10^{10}\,{\rm cm})$ is the disc size, measured from the centre of the accreting compact object, $\alpha = 0.1$ is the viscous parameters, $\dot{M}_{16} = \dot{M}/(10^{16}\,{\rm g\,s^{-1}})$ is the mass accretion rate and $m_1 = M/{\rm M}_\odot = 1.4$ is the compact object mass. In order to maximize $R_{10}$, we estimate the mass accretion rate from the maximum 0.01–100 keV X-ray luminosity (high count rate), $L_{\rm X} \sim 2.4\times10^{33}\,{\rm erg\,s^{-1}}$, and since $\dot{M} = L_{\rm X}/\eta\,c^2$ and $\eta = 0.1$ we get $\dot{M}_{16} \sim 2.7\times10^{-3}$. By imposing the viscous time-scale to be equal to the shortest correlation time-scale found, we can derive the maximum size of the disc for the specific time-scale. By using $t_{\rm c} \leq 110\,{\rm s}$ (correlation time-scale in the *U* band) we derive $R \lesssim 9\,{\rm km}$, a totally non-physical value, as it is smaller than the size of the NS itself. We note that also considering $\alpha = 1$ we get $R \lesssim 40\,{\rm km}$, which is once again a non-physical value, because the disc is not extending so close to the NS surface. We conclude that a standard disc cannot account for the observed correlation, implying that UV variability does not arise from instabilities propagating through a standard disc.

Finally, we also note that assuming that a BB and/or a disc BB model are reasonable approximations of the real disc spectrum, the temperatures derived from the SED fit for the inner disc edge is of the order of 16000–28000 K. At this temperature the disc would experience an immediate outburst (Menou & McClintock 2001, and references therein). So, the possibility that the UV is arising from a standard disc is also ruled out, in an independent way, based on the SED results.

### 5.4.3 *Advection dominated accretion flow*

According to Narayan & Yi (1995a,b), when the mass accretion rate, and the ratio *r*, drop below a critical (cr) value, $r_{\rm cr} = \dot{M}_{\rm cr}/\dot{M}_{\rm Edd}$, which in the case of an accreting NS if $\alpha = 0.1$ is $\sim 0.1\alpha^2 \sim 10^{-3}$, the accretion flow can only exhibit in two distinct stable states, namely the Shakura and Sunyaev thin disc and an ADAF. In ADAF the accretion flow is radiatively inefficient, and the energy produced by viscosity is advected by the flow and stored as heat, rather than being radiated away. Moreover, Narayan & Yi (1995b) also suggested that whenever $\dot{M} < \dot{M}_{\rm cr}$, the accretion flow always selects the ADAF solution, as it is the only really stable one. Independently of this last statement, we have already demonstrated that the standard disc cannot be the source of the observed UV variability. Since for Cen X-4 *r* is of the order of $10^{-6}$, we now explore the possibility that the correlation arises from an ADAF region, where UV flux variation could still trigger X-ray variation.

In an ADAF the matter moves towards the disc with a radial velocity $v_{\rm r} \sim \alpha\, c_{\rm s}$. The speed of sound is $c_{\rm s} \sim v_{\rm ff}$, where $v_{\rm ff} = ({\rm GM}/R)^{1/2}$ is the free fall velocity (Narayan & Yi 1995a). For a reasonable value of $\alpha$, $\sim$0.1, we have $v_{\rm r} = 0.1({\rm GM}/R)^{1/2}$. Since the time-scale at which accretion occurs is defined as $t_{\rm acc} = R/v_{\rm r}$, where *R* is the distance from the centre of the accreting object, we have

$$R = (t_{\rm acc}\,0.1)^{2/3}({\rm GM})^{1/3}. \quad (4)$$

We can estimate the maximum distance to the NS from which the matter is accreting in an ADAF ($R_{\rm acc}$), assuming that the accretion time-scale is equal to the shorter correlation time-scale we found ($t_{\rm cor} \leq 110\,{\rm s}$). This is a natural assumption since only if $t_{\rm acc} < t_{\rm cor}$ can accretion via an ADAF be the cause of the observed correlation. From equation (4), where $M = 1.4\,{\rm M}_\odot$, we get $R_{\rm acc} \lesssim 25000\,{\rm km}$, which corresponds to $\sim$6200 Schwarzschild radii, in agreement with theoretical values (Narayan & Yi 1995b). Consequently, the ADAF scenario can account for the time-scale of the correlation. The variability in the amount of matter that the star is accreting from a region inside of a radius of $R \sim 6200R_s$ could trigger X-ray variability. This radius must be considered as the maximum distance from which matter can be accreted on the NS in ADAF, based on the observed correlation. However, with present spectral data, we were unable to verify if the ADAF model can accurately reproduce the whole source SED (from optical to X-ray). The number of points in the *O* and *UV* band is limited to six, and the coverage is likely not wide enough. In fact, as already noticed by McClintock & Remillard (2000), the peak of the thermal synchrotron emission (*srcut* model used in the SED fit) depends on the mass of the compact object, $\nu_s \sim 10^{15}(M/{\rm M}_\odot)^{-1/2}$, and for any reasonable value of Cen X-4 NS mass, $\nu_s$ would lie well above the highest inspected frequency being $\nu_s > 6\times10^{15}$ Hz. However, instrumentally exploring higher frequency is not easily possible. On the other hand, Menou & McClintock (2001) modelled *Hubble Space Telescope* (*HST*)/STIS data of Cen X-4 with an ADAF plus a magnetosphere producing propeller effect. The magnetosphere complicates the scenario, likely truncating the innermost and hottest part of the accretion flow, where the brightest and high energetic (higher frequency) synchrotron emission should be generated. They argued that the synchrotron emission from an ADAF cannot account for the intensity and frequency peak of the observed UV emission and, consequently, concluded that for quiescent NS LMXB the contribution of an ADAF to the UV light must be very little. Summarizing, while the ADAF alone is very promising to explain the time-scale of the observed accretion, however, it seems to be unable to explain the intensity and the peak of the UV emission without invoking some still not well-understood extra effect.

### 5.4.4 *X-ray irradiation and reprocessing*

Another scenario proposed to explain the observed correlation takes into account the irradiation and reprocessing of the X-ray, arising

from (or near to) the NS surface, by part of the accretion disc (usually the inner part which will be hottest) as was suggested to explain the X-ray–UV correlation in Cen X-4 by Cackett et al. (2013a). We note that the light travel time from the NS to the outer edge of the disc is only about 5 s (the outer disc radius for a 15.1 h binary with an NS of 1.4 $M_\odot$ is $\sim 1.5 \times 10^{11}$ cm), so perfectly consistent with the reprocessing scenario.

The X-ray reprocessing from accretion disc was studied by van Paradijs & McClintock (1994) who found that the optical luminosity scales with the X-ray luminosity as $L_V \propto L_X^{1/2} R_{out}$, where $R_{out}$ is the radius of the outer accretion disc. This matches our results, as the most likely shape of the correlation is a power law, with index $\gamma$ always consistent, within $3\sigma$ of the statistical uncertainty, with 0.5.

Let us now explore in more detail the possibility that the X-rays are reprocessed by a standard disc at a radius $R$ from the NS surface. According to the reprocessing scenario the UV flux has to be only a small fraction of the X-ray one. More specifically, the maximum fraction of the reprocessed emission $S$ has to be equal to the fraction ($S'$) of the sphere surface of radius $R$ occupied by that part of the disc reprocessing the X-ray radiation. $S = S'$ only works if the reprocessing is 100 per cent efficient, otherwise $S < S'$. We emphasize that for a standard disc, $S'$ is always extremely small, as the disc is geometrically thin. In more detail, if $H$ is the vertical extension of the disc, we have $S' \simeq H/2R$. The ratio $H/R$ for a standard disc which is emitting because of irradiation, is given in Frank et al. (2002) as

$$H/R = 1.7 \times 10^{-2} \alpha^{-1/10} \dot{M}_{16}{}^{3/20} m_1^{-3/8} R_{10}^{2/7} f^{3/5}, \quad (5)$$

where $f = [1 - (R_{NS}/R)^{1/2}]^{1/4}$. $H/R$, and consequently $f$, are maximum at the outer disc (where $f \sim 1$ and $R = R_{10} \sim 15$, if $P = 15.1$ h). Since $\dot{M}_{16} \sim 2.7 \times 10^{-3}$ (see Section 5.4.2 for the estimate of $\dot{M}_{16}$), this implies that $S' \leq 0.8$ per cent. We stress that since $H/R \propto \dot{M}_{16}{}^{3/20}$, even if Cen X-4 was emitting at the Eddington limit, $S'$ would remain small, $\sim$5 per cent. However, the value of $S'$ does not match the amount of UV reprocessing estimated from the observation, where $S = F_{UV}/F_X$ is $2.1 < S < 23$ per cent (see Section 4.6). We therefore conclude that 2.1–23 per cent is not a reasonable value for reprocessed emission from a standard thin disc (note that this is in contrast to the conclusions of Cackett et al. 2013a, who did not fully consider the geometric size of disc). Our conclusions are even stronger if we take into account only the inner edge of the disc where H/R is minimal. We note that in order to have $F_{UV}/F_X \leq 0.8$ per cent, as the observed UV flux is $1.06 \times 10^{-12}$ erg cm$^{-2}$ s$^{-1}$ ($L_{UV} = 1.83 \times 10^{32}$ erg s$^{-1}$), the 0.01–100 keV X-ray flux should be $F_X \geq 1.3 \times 10^{-10}$ erg cm$^{-2}$ s$^{-1}$ ($L_X \geq 2.2 \times 10^{34}$ erg s$^{-1}$). This is well above the maximum quiescent luminosity ever recorded from the source.

We emphasize that, however, the real structure of the disc in quiescence is unknown, and it is likely different from the standard disc configuration. For example, the value $\alpha$ could depend on the radius $R$ (while the standard disc solution assumes that $\alpha$ is constant), and this can make the scenario more complex. Among other things, the vertical size of the outer disc could be greater than envisaged in simplified treatments of the inner disc. In any case, in order to be the disc alone to reprocess, e.g. 5 per cent of the X-ray emission, its vertical size must be $H \geq 10$ per cent $R$. Any disc model invoked to account for reprocessing must be able to account for that.

On the contrary, we note that the fraction of the sphere of radius $R$ occupied by the surface of the companion star of radius $R_c$ is consistent with the observed fraction of reprocessed light. Indeed, in this case $S' \simeq 1/2(R_c/R)^2$. The companion star is a K3–7 V star with radius $0.5 < R_c/R_\odot < 1.2$, and that the mass ratio of Cen X-4 is $q = 0.17 \pm 0.06$. By using the Eggleton's equation we can derive the ratio $R_c/R = 0.49q^{2/3}/[0.6q^{2/3} + \ln(1 + q^{1/3})]$. Taking into account the $1\sigma$ uncertainty on the measure of $q$ we get $2.3 < S' < 3.4$ per cent, which matches our experimental results. We conclude and stress that the companion star is the most likely source of reprocessing, while the accretion disc alone cannot.

We emphasize that the SED, in addition to the emission from the companion star, also indicates the presence of a small ($\sim 2.4 \times 10^4$ km) hot ($kT \sim 0.0014$ keV and $\sim$16 000 K), thermally emitting region, that we demonstrated is not the accretion disc. This could be a hotspot on the star companion, which is likely hotter because it is directly (without any shield from the accretion disc) irradiated by the X-ray photons. However, a higher number of data points in the *UV* band (compared to our four) is mandatory to properly characterize this component. The $3\sigma$ upper limit on the size of the spot is about 43000 km. This corresponds to a fractional surface area of about 2 per cent for a 0.5 $R_\odot$ companion (that is the companion radius estimated from the SED fit). We note that this UV component has a small area. However, we used a simple BB model to fit for something which is likely more complex. Moreover, we can speculate that the X-ray reprocessing is likely generating a gradient of temperature over the companion star. Due to the limited number of points (4) in this band we can highlight and measure only where this gradient is maximum, likely a small region closer to the NS.

Torres et al. (2002) argued that the X-ray irradiating the inner face of the companion star can generate a narrow H$\alpha$ line detected in the optical spectrum. Furthermore, the contribution in the optical of a hotspot on the companion star due to X-ray heating is required to model the optical and IR light curve of Cen X-4 (McClintock & Remillard 1990; Shahbaz et al. 1993). More recently, accurate Doppler tomography of Cen X-4 was performed by D'Avanzo et al. (2005). They found strong H$\alpha$ and He I ($\lambda$5876 Å) emission from the companion due to irradiation from the NS. Moreover, they even found the outer disc to be irradiated. Indeed the outer disc is hotter than the companion, emitting optical He I ($\lambda$6678 Å) lines. They argue that the H$\alpha$ emission from the secondary originated in a region close to the Lagrangian point, where the X-ray radiation is mainly occulted by the disc, and consequently this region is cooler, while the He I ($\lambda$5876 Å) might arise from the portion of the companion star surface which is directly irradiated by the X-ray (not blocked by the disc), and hence this region is hotter. All these results support the idea of a hotspot on the star due to X-ray irradiation.

We also found a correlation between the X-ray and the optical *V*-band emission. This was not seen in Cackett et al. (2013a) where they have significantly fewer points, and is only revealed here by the much larger data set and dynamic range in X-ray flux. If we compare the constant plus power-law model to fit for the shape of the correlation in the case of the *V* band ($t \leq 5$ and $\leq$2 ks), with that of the *UV* bands, we note that while for a low X-ray count rate the UV count rate goes extremely close to zero, this is not the case for the *V* band. This suggests that there is an intrinsic level of emission in the *V* band, independently of the physical mechanism causing the correlation, and it is much higher than that in the *UV* bands. We now estimate, for each band, the ground level of emission and its contribution to the total light. We measure the value of the constant in the fit which is 0.5 c s$^{-1}$ in the *V* band compared to a $3\sigma$ upper limit of 0.02 c s$^{-1}$ in the case of the *UVW1* band. We note that 0.5 c s$^{-1}$ is exactly the ground level from which the *V* band light curve displays its variability (see Fig. 1). Taking into

account that the maximum $V$ count rate is $\sim 0.8\,\mathrm{c\,s^{-1}}$, this corresponds to a 60 per cent increase from $0.5\,\mathrm{c\,s^{-1}}$. This means that at least 40 per cent of the total emission in the $V$ band, is stable, and likely due to the companion star which, indeed, is expected to dominate at optical wavelengths (Chevalier et al. 1989). However, part of the intrinsic $V$ emission can also arise from the accretion disc, but with present data we cannot quantify it (Chevalier et al. 1989, estimated a 25 per cent contribution in the $V$ band due to the disc), while Shahbaz et al. (1993) estimated a 10 per cent contribution in the IR. Concerning the *UVW*1 band, the maximum count rate is $0.7\,\mathrm{c\,s^{-1}}$, this corresponds to an increase by a factor of $\sim$34 compared to the ground level. This implies that the intrinsic emission in this band must be lower than 3 per cent.

Following our analysis for the X-ray and UV fluxes, we can also measure the ratio between X-ray and optical fluxes. However, we only consider here the variable optical flux ($3 \times 10^{-13}\,\mathrm{erg\,cm^{-2}\,s^{-1}}$, about 60 per cent of the total). Taking into account the uncertainty on the X-ray flux measurement the resulting ratio is $0.6 < F_{\rm O}/F_{\rm X} < 6.5$ per cent. We conclude that also the variable optical emission is likely due to reprocessing from the companion star.

Summarizing, we conclude that the accretion disc must be intrinsically faint in the UV during quiescence, with a maximum of 3 per cent of the total light in this band arising from it, while, it can be brighter in the optical band. This is in agreement with the conclusion of Torres et al. (2002) that suggested that the companion has a comparable luminosity in the optical (H$\alpha$) than the accretion disc and is brighter at shorter wavelengths. This is also in agreement with the analysis of Reynolds et al. (2008) that with the goal of understanding the nature of a near-infrared excess in the emission from a sample of X-ray novae, hosting both BH and NS, including Cen X-4, found that the component required to match the observed excess is consistent with a disc truncated at $10^3$–$10^5 R_{\rm s}$, with an irradiated temperature profile in all cases (i.e. $T(r) \sim r^{-0.5}$). A standard steady state temperature profile is unable to account for the observed excess. Such kind of disc will contribute only minimally in the UV. We also conclude that almost all the variable UV emission, which represents $\sim$100 per cent of the total emission in these bands, must arise from reprocessing from the surface of the companion facing the NS. Also part of the variable optical ($V$) emission, that represents $\sim$60 per cent of the total in the band, must arise from reprocessing, while another part can arise from orbital modulation. By folding the $V$ and *UVW*1 light curves at the 15.1 orbital period, we measured a 6 and 10 per cent $3\sigma$ upper limit due to the orbital contribution, respectively (however, Chevalier et al. 1989, with higher S/N data, measured the $V$ flux variation due to orbital 15.1 h modulation to be $\sim$17 per cent). Moreover, we also found that the X-ray irradiation is likely generating on the surface of the companion a small ($\sim$2 per cent of the whole surface for a $0.5\,\mathrm{R_\odot}$ companion) hotspot.

Finally, we emphasize that the ADAF and reprocessing scenario are not mutually exclusive, they in fact could easily coexist. Indeed, most if not all the UV emission is produced by reprocessing from the companion star, as we have shown, it is not surprising that the ADAF model alone cannot account for the intense emission in the *UV* band (as suggested by Menou & McClintock 2001). We note that, at least for what concerns Cen X-4, a detailed model including ADAF plus reprocessing from the companion should be tested against the data. We have demonstrated that matter must accrete on the NS surface, and the fact that this matter can be in an ADAF state is not in contrast with our results.

We emphasize that the estimate of the ratio $F_{\rm UV}/F_{\rm X}$ depends on the exact slope of the hard power-law tail. New simultaneous observations performed e.g. with *NuSTAR* and *Swift* (or *XMM–Newton* or *HST*) will certainly allow us to firmly measure the slope and the flux of the power law (*NuSTAR*) together with the simultaneous flux in the optical and *UV* bands (*Swift* or *HST* or *XMM–Newton*). This will constrain the ratio $F_{\rm UV}/F_{\rm X}$. If this ratio will be well above 4.7 per cent,[6] a different scenario from reprocessing should be considered. Indeed, no other optically thick surfaces are present in the binary system other than the disc and the companion star. The only plausible alternative to it, is that the accreting matter is intrinsically emitting in the UV. The specific ADAF model for this system should be produced accordingly.

## 6 SUMMARY

We analysed 60 multiwavelength (O, UV and X-ray) simultaneous observations of Cen X-4, performed by the *Swift* observatory on a daily basis, with the goal to learn from the source quiescent variability about the emission mechanisms powering the optical, UV and X-ray emission. The main result of this work can be summarized as follows.

The optical, UV and X-ray quiescent light curves are strongly variable both on short (days) and on long (months) timescales as is showed by their first-order structure function. The X-ray band is more variable than the *UV* and the optical band, meaning that the amplitude of the variability is higher, as also pointed out by the fractional root-mean-square variability which is $F_{\rm var}^{\rm X-ray} = 73.0 \pm 1.5$ per cent, $F_{\rm var}^{\rm UVW1} = 50.0 \pm 1.4$ per cent and $F_{\rm var}^{V} = 10.0 \pm 1.6$ per cent. We observed the strongest short timescale X-ray, flare-like, variability ever recorded from Cen X-4 in quiescence: a factor of 22 drop in only 4 d.

We found a highly significant and strong correlation between the X-ray and the UV (*UVW*2, *UVM*2, *UVW*1 and *U*) emission on long time-scale ($t \leq 5$ ks), on short time-scale ($t \leq 2$ ks) and also on very short time-scale (down to $t \leq 110$ s). We found a significant but less intense correlation also between the X-ray and the $V$ band on long time-scale ($t \leq 5$ ks), and on short time-scale ($t \leq 2$ ks). No significant correlation was detected with the $B$ band, likely because the limited number of pointings performed in this band and the consequent lack of coverage at high X-ray count rate. The most likely shape of the correlation is a power law with index $\Gamma = 0.2$–0.6.

We produced three averaged X-ray spectra as a function of the source count rate, low $<0.07\,\mathrm{c\,s^{-1}}$, medium 0.07–$0.11\,\mathrm{c\,s^{-1}}$ and high $>0.11\,\mathrm{c\,s^{-1}}$. We found the spectra well fitted by a model made by the sum of a thermal component in the form of hydrogen NS atmosphere plus a non-thermal power-law tail, both multiplied by the interstellar absorption. Both components must change with the flux. The overall spectral shape remains the same with respect to flux variability as we show by both count rate and spectral analysis. The thermal and the power-law component are changing in tandem, being both responsible always for the same fraction, about 50 per cent, of the total X-ray flux in the 0.5–10 keV band. This suggests that they are physically linked. The temperature of the NS surface is changing being hotter when the flux is higher: $kT_{\rm h} = 80 \pm 2$ eV, $kT_{\rm m} = 73.4 \pm 0.9$ eV and $kT_{\rm l} = 59.0 \pm 1.5$ eV (while $\Gamma_{\rm h} = 1.4 \pm 0.5$, $\Gamma_{\rm m} = 1.4 \pm 0.2$, $\Gamma_{\rm l} = 2.0 \pm 0.2$). We conclude that accretion is very likely still occurring also at low Eddington luminosity rates ($\sim 10^{-6}$) and that the matter is reaching

[6] Considering the $3\sigma$ uncertainty on the mass ratio $q \lesssim 0.29$, consequently, $F_{\rm UV}/F_{\rm X} \lesssim 3.9$ per cent. By including also the maximum contribution from the accretion disc 0.8 per cent we get a total of about 4.7 per cent.

and heating the NS surface, overtaking the action of the centrifugal force of the rotating magnetosphere. Since the two spectral components are closely linked, accretion is likely generating somehow also the power-law component.

We demonstrated that the UV emission cannot be thermal emission from the gas stream impact point. This scenario cannot account for the time-scale of the observed X-ray and UV correlation. The UV emission can arise neither from matter moving inward in a standard optically thick nor from geometrically thin accretion disc. Indeed, due to the short time-scale of the correlation the matter should move from a starting point at a maximum distance of about 30 km from the star centre. However, the disc is very likely not extending so close to the surface, otherwise it would shine in the X-ray, moreover, it has never been observed in the X-ray quiescent spectrum of Cen X-4. The UV emission is not even produced by reprocessing from a standard thin disc. Indeed, the fraction of UV versus X-ray flux is too high (in the range 2.1–23 per cent), as the maximum allowed reprocessing fraction from a standard disc is lower than 0.8 per cent. We found, on the contrary, that most (if not all) the UV emission and part (∼60 per cent) of the optical emission is very likely generated by reprocessing from the whole surface of the companion star. Moreover, we found indication of the presence of a small hotspot (∼16 000 K, $\sim 2.4 \times 10^4$ km, fractional area of about 2 per cent) on the companion star which could be generated by X-ray irradiation, likely in a region where no shield is provided by the accretion disc. We found that the accretion disc must be UV faint, as its contribution to the total UV light is less than 3 per cent (but it can still be optically bright).

We have shown that a strong propeller-type outflow powered by the interaction with the accretion flow and the stellar magnetic field is very unlikely to be present in Cen X-4, as is required for the ADAF propeller scenario. A strong outflowing wind (ADIOS) solution could be instead favoured. However, a 'dead disc' may also form in the inner regions of the accretion flow, which inhibits but does not completely prevent accretion on to the star, allowing accretion to proceed even at rates when the 'propeller' solution would otherwise be active.

The time-scale of the correlation could suggest that the accreting matter can be in an ADAF state, which is likely UV faint, at a distance less or equal to $\sim 6200\, R_s$. However, the spectral analysis (SED) does not confirm the presence of an ADAF. We have only tested separate reprocessing and ADAF models, however, it could be that both processes are involved. A more detailed model including both an ADAF and reprocessing on the companion star should be developed and tested against these data.

## ACKNOWLEDGEMENTS

FB thanks Aron Zell and Jean Charles Tropato for their precious help, and Ramesh Narayan for the useful discussion. ND is supported by NASA through Hubble Postdoctoral Fellowship grant number HST-HF-51287.01-A from the Space Telescope Science Institute. RW acknowledges support by an European Research Council Starting Grant.

## REFERENCES

Armas Padilla M., Degenaar N., Wijnands R., 2013, MNRAS, 434, 1586
Arnaud K. A., 1996, in Jacoby G. H., Barnes J., eds, ASP Conf. Ser. Vol. 101, Astronomical Data Analysis Software and Systems V. Astron. Soc. Pac., San Francisco, p. 17
Asai K., Dotani T., Hoshi R., Tanaka Y., Robinson C. R., Terada K., 1998, PASJ, 50, 611
Blandford R. D., Begelman M. C., 1999, MNRAS, 303, L1
Breeveld A. A. et al., 2010, MNRAS, 406, 1687
Brown E. F., Bildsten L., Rutledge R. E., 1998, ApJ, 504, L95
Brown E. F., Bildsten L., Chang P., 2002, ApJ, 574, 920
Cackett E. M., Wijnands R., Miller J. M., Brown E. F., Degenaar N., 2008, ApJ, 687, L87
Cackett E. M., Brown E. F., Miller J. M., Wijnands R., 2010a, ApJ, 720, 1325
Cackett E. M., Brown E. F., Cumming A., Degenaar N., Miller J. M., Wijnands R., 2010b, ApJ, 722, L137
Cackett E. M., Fridriksson J. K., Homan J., Miller J. M., Wijnands R., 2011, MNRAS, 414, 3006
Cackett E. M., Brown E. F., Degenaar N., Miller J. M., Reynolds M., Wijnands R., 2013a, MNRAS, 433, 1362
Cackett E. M., Brown E. F., Cumming A., Degenaar N., Fridriksson J. K., Homan J., Miller J. M., Wijnands R., 2013b, ApJ, 774, 131
Campana S., Stella L., 2000, ApJ, 541, 849
Campana S., Mereghetti S., Stella L., Colpi M., 1997, A&A, 324, 941
Campana S., Israel G. L., Stella L., Gastaldello F., Mereghetti S., 2004, ApJ, 601, 474
Cannizzo J. K., 1993, in Wheeler J. C., ed., The Limit Cycle Instability in Dwarf Nova Accretion Disks. World Scientific Press, Singapore, p. 6
Cardelli J. A., Clayton G. C., Mathis J. S., 1989, ApJ, 345, 245
Chevalier C., Ilovaisky S. A., van Paradijs J., Pedersen H., van der Klis M., 1989, A&A, 210, 114
Conner J. P., Evans W. D., Belian R. D., 1969, ApJ, 157, L157
D'Angelo C. R., Spruit H. C., 2010, MNRAS, 406, 1208
D'Angelo C. R., Spruit H. C., 2012, MNRAS, 420, 416
D'Avanzo P., Campana S., Casares J., Israel G. L., Covino S., Charles P. A., Stella L., 2005, A&A, 444, 905
Degenaar N., Wijnands R., 2012, MNRAS, 422, 581
Degenaar N. et al., 2011a, MNRAS, 412, 1409
Degenaar N., Brown E. F., Wijnands R., 2011b, MNRAS, 418, L152
Dickey J. M., Lockman F. J., 1990, ARA&A, 28, 215
Do T., Ghez A. M., Morris M. R., Yelda S., Meyer L., Lu J. R., Hornstein S. D., Matthews K., 2009, ApJ, 691, 1021
Frank J., King A., Raine D. J., 2002, Accretion Power in Astrophysics, 3rd edn. Cambridge Univ. Press, Cambridge
Fridriksson J. K. et al., 2011, ApJ, 736, 162
Gehrels N. et al., 2004, ApJ, 611, 1005
Ghosh P., Lamb F. K., 1979, ApJ, 234, 296
González Hernández J. I., Rebolo R., Israelian G., Casares J., Maeda K., Bonifacio P., Molaro P., 2005, ApJ, 630, 495
Güver T., Özel F., 2009, MNRAS, 400, 2050
Heinke C. O., Rybicki G. B., Narayan R., Grindlay J. E., 2006, ApJ, 644, 1090
Heinke C. O., Jonker P. G., Wijnands R., Taam R. E., 2007, ApJ, 660, 1424
Heinke C. O., Jonker P. G., Wijnands R., Deloye C. J., Taam R. E., 2009, ApJ, 691, 1035
Hughes P. A., Aller H. D., Aller M. F., 1992, ApJ, 396, 469
Hynes R. I., Robinson E. L., 2012, ApJ, 749, 3
Illarionov A. F., Sunyaev R. A., 1975, A&A, 39, 185
Kalberla P. M. W., Burton W. B., Hartmann D., Arnal E. M., Bajaja E., Morras R., Pöppel W. G. L., 2005, A&A, 440, 775
Kaluzienski L. J., Holt S. S., Swank J. H., 1980, ApJ, 241, 779
Kubota A., Tanaka Y., Makishima K., Ueda Y., Dotani T., Inoue H., Yamaoka K., 1998, PASJ, 50, 667
Kuulkers E., in't Zand J. J. M., Lasota J.-P., 2009, A&A, 503, 889
Lasota J.-P., 2001, New Astron. Rev., 45, 449
Lii P. S., Romanova M. M., Ustyugova G. V., Koldoba A. V., Lovelace R. V. E., 2013, preprint (arXiv:1304.2703)
Matsuoka M. et al., 1980, ApJ, 240, L137
McClintock J. E., Remillard R. A., 1990, ApJ, 350, 386
McClintock J. E., Remillard R. A., 2000, ApJ, 531, 956
Menou K., McClintock J. E., 2001, ApJ, 557, 304

Menou K., Esin A. A., Narayan R., Garcia M. R., Lasota J.-P., McClintock J. E., 1999a, ApJ, 520, 276
Menou K., Esin A. A., Narayan R., Garcia M. R., Lasota J.-P., McClintock J. E., 1999b, ApJ, 520, 276
Narayan R., Yi I., 1995a, ApJ, 444, 231
Narayan R., Yi I., 1995b, ApJ, 452, 710
Narayan R., Mahadevan R., Quataert E., 1998, in Abramowicz M. A., Bjornsson G., Pringle J. E., eds, The Theory of Black Hole Accretion Discs. Cambridge Univ. Press, Cambridge, p. 148
Poole T. S. et al., 2008, MNRAS, 383, 627
Reynolds M. T., Callanan P. J., Robinson E. L., Froning C. S., 2008, MNRAS, 387, 788
Roming P. W. A. et al., 2005, Space Sci. Rev., 120, 95
Rutledge R. E., Bildsten L., Brown E. F., Pavlov G. G., Zavlin V. E., 1999, ApJ, 514, 945
Rutledge R. E., Bildsten L., Brown E. F., Pavlov G. G., Zavlin V. E., 2001, ApJ, 551, 921
Rutledge R. E., Bildsten L., Brown E. F., Pavlov G. G., Zavlin V. E., 2002, ApJ, 577, 346
Shahbaz T., Naylor T., Charles P. A., 1993, MNRAS, 265, 655
Shakura N. I., Sunyaev R. A., 1973, A&A, 24, 337
Soria R., Zampieri L., Zane S., Wu K., 2011, MNRAS, 410, 1886
Spruit H. C., Taam R. E., 1993, ApJ, 402, 593
Torres M. A. P., Casares J., Martínez-Pais I. G., Charles P. A., 2002, MNRAS, 334, 233
Tsujimoto M. et al., 2011, A&A, 525, A25
van Paradijs J., McClintock J. E., 1994, A&A, 290, 133
Vaughan S., Iwasawa K., Fabian A. C., Hayashida K., 2005, MNRAS, 356, 524
Verner D. A., Ferland G. J., Korista K. T., Yakovlev D. G., 1996, ApJ, 465, 487
Wijnands R., Degenaar N., 2013, MNRAS, 434, 1599
Wijnands R., Degenaar N., Page D., 2013, MNRAS, 432, 2366
Zampieri L., Turolla R., Zane S., Treves A., 1995, ApJ, 439, 849
Zurita C., Casares J., Shahbaz T., 2002, in Gänsicke B. T., Beuermann K., Reinsch K., eds, ASP Conf. Ser. Vol. 261, The Physics of Cataclysmic Variables and Related Objects. Astron. Soc. Pac., San Francisco, p. 573

This paper has been typeset from a TEX/LATEX file prepared by the author.